# Improvement of fatigue and corrosion-fatigue resistance of AZ31B cast alloy by cold spray coating and top coating

by

Siavash Borhan Dayani

A thesis

presented to the University of Waterloo

in fulfilment of the

thesis requirement for the degree of

Master of Applied Science

in

Mechanical and Mechatronics Engineering

Waterloo, Ontario, Canada, 2017

## Author's Declaration

I hereby declare that I am the sole author of this thesis. This is a true copy of the thesis, including any required final revisions, as accepted by my examiners.

I understand that my thesis may be made electronically available to the public.

# Abstract

Recent advancements in manufacturing of light-weight structures have caused high interest in industries toward magnesium alloys because of its excellent properties such as specific strength, low density, and fatigue strength. Application of magnesium in the vehicle structure saves energy and reduces gas emission which consequently improves the performance of the vehicle. Magnesium alloys have low corrosion resistance and high tendency to corrode in humid and aqueous environments. The results of recent research show that cold spray coating of pure aluminium powder results in significant improvement in magnesium corrosion. However when tested under cyclic loads, the coated samples developed surface cracks and delamination. Which lead to highly localized corrosion damages underneath of the cracks or any discontinuity in the components. The early cracking was attributed to the low fatigue resistance of pure aluminium.

The results of two new approaches in enhancing the corrosion fatigue life of coated magnesium are presented in this thesis. First, an aluminium alloy coating powder with the higher fatigue strength was selected for coating. Al-7075 powder, with average particle size of twenty microns have successfully been coated on AZ31B samples with highly densed, low porosity coated layer. The coating was performed using nitrogen gas at 400oC temperature, and gas pressure of 200 psi. Electrostatic painting was then applied. Result of tests in the corrosive atmosphere of 3.5 % of NaCl solution as well as rotating fatigue test in corrosive environment will be presented. Improvement of fatigue resistance of cold spray coated samples and corrosion-fatigue resistance of cold spray coated, e-painted samples are studied in this thesis.

## Acknowledgements

*To my family that I could perform*

*this thesis by their kindly supports*

# Table of Contents

# List of Figures

# List of Tables

# Chapter 1   Introduction

## 1.1 Motivation

Over the course of history, human civilization progressed as a direct result of advancements in science and technology, such as the discovery of new places, new materials, and improved methods for our activities. For example, the Stone Age ended not because stone resources were depleted, but because of the discovery of materials that were superior to stone; it was followed first by the Bronze Age, then by the Iron Age.  Steel, the main alloy of iron, is now the most frequently used alloy in the world and is used in vast number of different industries. However, in recent decades, considerable attention has been paid to other materials. Steel is cost-effective, easy to machine, and relatively abundant, but it has a high density. Lighter alternatives to steel are increasingly receiving more attention. The strength to density ratio (specific strength) for some of the widely used material is presented in Figure 1–1, and the machinability of metals and alloys is presented in Figure 1–2.
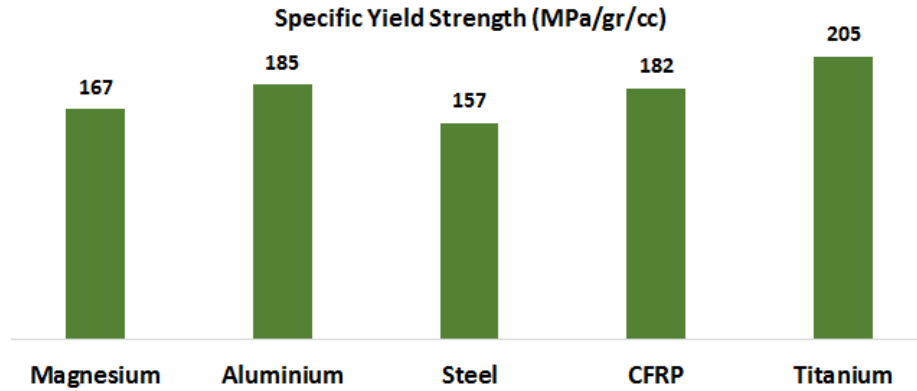
**Figure 1–1: Specific yield strength of five usual metals or alloys [1]**
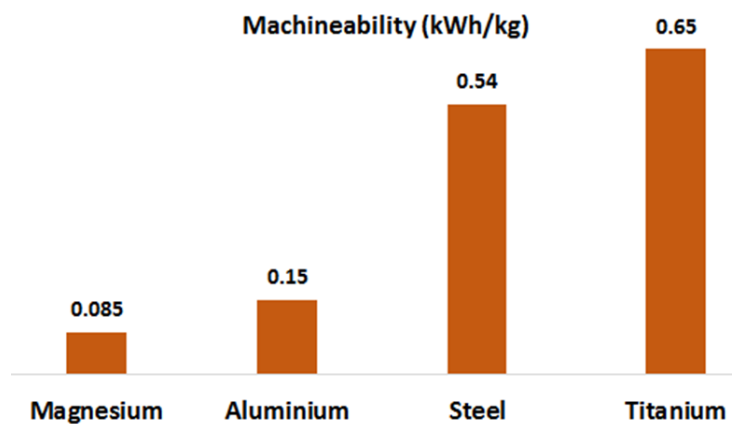


**Figure 1–2: Machinability required power of four metals or alloys [1]**

The combination of low machining cost, and high specific strength, and low density (1738 kg/m³) has made magnesium alloy highly attractive for light weighting. The use of a light magnesium alloy instead of alternative alloys like steel leads to a weight reduction of more than twenty percent [2]. Recently, there has been an emerging interest in the study of the mechanical properties of magnesium alloys for use in transportation systems [3]. Magnesium fatigue properties are of particular interest for applications in automotive structural parts that are under cyclic loading. A focus of this research is the development of methods to improve fatigue resistance of a magnesium alloy.

Equally important to fatigue resistance is corrosion resistance and the effect of a corrosive environment on vehicle parts. Corrosion resistance of a material becomes

more important when the material is a magnesium alloy, which has a higher corrosion tendency than other alloys like steel. Another focus of this research is to improve corrosion resistance while improving fatigue strength. Aims of this research include the improvement of both features. The key word used frequently in this thesis is *corrosion-fatigue resistance*, which defines the resistance of the material against cyclic loading in a corrosive environment.

Cold spray coating is a new technology that deposits metal powder onto a substrate at a low temperature. The mechanical bond between the powder and the substrate is formed because of supersonic speed of the powder particles and the local plastic deformation due to the high impact. As a result, compressive stresses are induced, which in turn delay crack initiation and improve fatigue resistance [4]. This effect is defined in some references as the peening effect [5]. In addition to the peening effect, the surface is covered by a new material which, if stronger, will prevent crack initiation on the substrate surface. Cold spray coating can then have a positive effect on improving fatigue resistance. Cold spray coating, depending on the coating material, provides many advantages, such as: no oxidation, no phase change, low porosity, good bonding strength, compressive residual stress, possibility to spray on thermal sensitive substrates, possibility to produce thick deposits (additive fabrication), well-defined spraying spot, requirement for minimum surface preparation, simple operation, no combustion fuels, and no plasma requirement. Aluminum 7075 powder, with high hardness and ultimate strength, was selected for coating AZ31B cast in this research. Beside residual stress improvement, corrosion protection was also of interest in selecting aluminium powder. An industrial top coating (e-paint) was selected to improve corrosion-fatigue resistance. Performance tests on the prepared samples for evaluating corrosion-fatigue resistance of the processed samples were the next steps of the research for verification of the methods.

The objectives of this research were:

1) To development cold spray coating of Al7075 on AZ31B cast substrate

2) To characterize the developed coat

3) To identify and apply a suitable top-coat for improving corrosion resistance

4) To characterize fatigue and corrosion-fatigue behaviour of coated samples

## 1.2 Thesis organization

This thesis consists of five chapters. Chapter One describes the motivation and objectives of this research work and presents an overview of the thesis. Chapter Two presents a thorough review of the literature that pertains to this work. It includes recent researches on the fatigue resistance of AZ31B, cold spray on magnesium alloys, cold spray of Al7075 powder, and fatigue and corrosion-fatigue performance of cold spray coated samples.

Chapter Three describes the experiments performed, and the equipment used. This chapter includes an explanation of the cold spray system in detail, as well as explanations of the selection of the coating material, characterization of the coating powder, first cold spray coating trials and the parameters used in the coating processes, and the process performed for flat samples and round samples. Details of performance tests, such as tension test, hardness test, and residual stress measurement are also provided in Chapter Three.

Chapter Four presents the effect of cold spray process on fatigue resistance and the fatigue tests. S-N curves and fracture surface analysis are presented in this chapter. A detailed comparison of the performance of the two groups of samples: bare samples and cold spray coated samples, is given.

Chapter Five outlines the top coating process and reviews its effect on corrosion-fatigue performance of cold spray coating. The results of four corrosion-fatigue tests on bare, bare-top coat, cold spray coated, and cold spray coated with top coat are presented and discussed in detail in this chapter. Analysis of the fracture surfaces of these tests and sources of failure are also presented.

Chapter Six presents conclusions, recommendations and future research related to the problems and new ideas of the processes. The difference of fatigue resistance in different prepared samples and the method to figure out the reason are the gaps need to be covered. Research on other coating material and their performance is recommended in the last chapter.

# Chapter 2   Literature review

## 2.1 Necessity of weight reduction and light alloys

Recent advancements in manufacturing of light-weight structures have led to substantial interest from industry in magnesium alloys because of their desirable properties such as high specific strength and specific stiffness, and low density [6]. The weight of components and vehicles is the main factor that determines vehicle resistance forces in transportation industries. Friction forces, acceleration forces, braking forces, and other resistances will decrease with decreasing weight of the components and vehicles in all types of transportation. Table 2-1 presents a comparison of resistance forces of vehicles under different loading conditions [7]. Obviously, higher levels of resistance require higher rates of energy consumption and fuel usage in vehicles. Table 2-2 presents approximate fuel consumption values of some transportation devices.

Table 2-1: Resistance force of vehicle regarding to vehicle weight [7]

| Weight of the vehicle | Rolling resistance | Traction force in 2 m/s² acceleration | Resistance force in 6 ° slope (constant speed) |
|---|---|---|---|
| 500 kg | 50 ~ 70 N | 1000 N | 512 N |
| 1500 kg | 120 ~ 200 N | 3000 N | 1536 N |
| 5000 kg | 400 ~ 600 N | 10000 N | 5120 N |
| 10000 kg | 1000 ~ 1500 N | 20000 N | 10240 N |

Table 2-2: Fuel consumption of transportation system in different weight

| Transportation device | Rough fuel consumption |
|---|---|
| Motorcycle [8] (200 kg) | 2 liters/ 100 km of gasoline |
| Small boat [9] (300 kg) | 10 liters/ 100 km of gas oil |
| Passenger car [10] (1000 kg) | 9 liters/ 100 km of gasoline |
| Fishing ship [9] (15 metric ton | 600 liters/ 100 km of gas oil |
| Diesel truck [11] (5 metric ton) | 15 liters/ 100 km of gas oil |
| Diesel truck [11] (30 metric ton) | 50 liters/ 100 km of gas oil |

The side effects of huge amounts of fossil fuel consumption, in both the short term and long term, locally and globally, economically and environmentally, are significant and numerous. Global warming, air pollution, depletion of natural resources, and increases in energy prices, are some examples of the effects of widespread fossil fuel-based energy consumption. Reducing the amount of energy consumption by even a small percentage leads to positive effects on the environment. The use of light alloys of magnesium and other light metals in place of heavier material is a promising and attractive approach to reducing vehicle weight, and thereby energy consumption, in transportation industries. Research suggests the possibility of 20 % reduction in the overall weight of vehicles if magnesium alloys are used to replace

certain components made of steel. [2]. Increasing the usage of magnesium is the subject of a considerable amount of research in this field [3].

## 2.2 AZ31B cast alloy

Since magnesium alloys have very good castability, they are used often for casting and die-casting applications. AZ, AM, AS, and AE alloys are the four main groups of magnesium casting alloys [1]. Table 2-3 presents the alloying elements' indices for magnesium alloys.

**Table 2-3: Indices of alloying elements in magnesium alloys [1]**

| Letter | Alloying elements |
|--------|-------------------|
| A | Aluminum |
| C | Copper |
| E | Rare earth metals |
| H | Thorium |
| K | Zirconium |
| L | Lithium |
| M | Manganese |
| Q | Silver |
| S | Silicon |
| Y | Yttrium |
| Z | Zinc |

Regarding the alloying elements, wrought alloys have different mechanical properties [12]. The yield strength and ultimate strength increase considerably as a result of extrusion, while the behaviour of extruded Mg alloys become anisotropic. Regarding the low number of additional elements, AZ31B is the subject of attention because of its low cost in comparison to other magnesium alloys [1]. AZ31B as cast billets, extruded billets, and rolled sheet are most frequent forms of this alloy. A comparison of isotropy behaviour of magnesium alloy has been performed which shows that cast magnesium alloys have isotropic behavior [13]. Because of their low cost, high strength, and desirable isotropic behaviour, these three types of AZ31B alloys are used widely. For this research, cast alloy has been selected. A brief review of the mechanical properties of AZ31B is covered. The main focus of most related research is

on extruding alloys, while in this study, the properties of AZ31B cast alloy, required to use the alloy in the industry are investigated.

## 2.3 Fatigue properties of AZ31B

In transportation systems, many of the components persist cyclic loads because of the road profile and cyclic loads of the rotational components [14]. Regarding the movement of the parts in transportation systems such as reciprocation, rotation, transferring of the loads caused by road unevenness, etc., the parts are under cyclic loading and fatigue, and the main cause of failure in these parts is fatigue failure. Light alloys have received attention from automotive companies for applications in suspension and axle parts, which are under cyclic loading [15]. As explained above, research on fatigue resistance of AZ31B and its improvement is attractive for transportation industry to facilitate the usage of this alloy. The fatigue resistance of AZ31B has been studied by Tokaji et al. [16]; they indicate that the fatigue limit for ten million cycles is 50 MPa. Figure 2–1 shows the S-N curve of AZ31B they prepared.
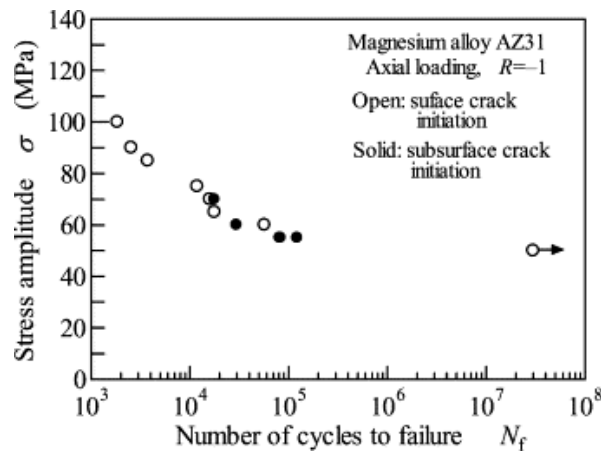


**Figure 2–1: S-N curve of AZ31B [16]**

Kim et al. [16] in 2004 presented the results of research on fatigue behaviour of AZ31B and the effect of grain size on fatigue properties of AZ31B. They present the relationship between fatigue limit and grain size. The fatigue resistance of different types of AZ31B extrude alloy has been compared by Chino et al. [18]; they indicate that

the limits for recycled alloy and received alloy were 95 MPa and 120 MPa, respectively.

Figure 2–2 represents the S-N curve of AZ31B they prepared.
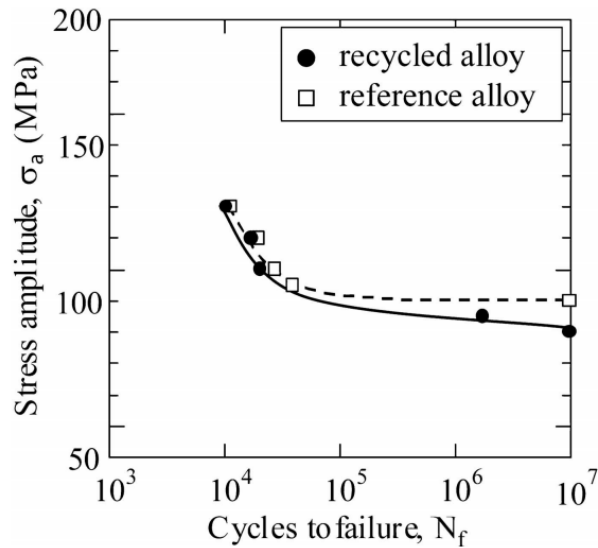


**Figure 2–2: S-N curve of AZ31B [18]**

A corrected Coffin-Manson model of AZ31B extrude has been presented by Hasegawa et al. [19] in 2007 and is shown in Figure 2–3. Ishihara et al. [20] demonstrated higher fatigue resistance of extrude samples that are parallel to the extrusion direction, compared to those perpendicular to the extrusion direction.
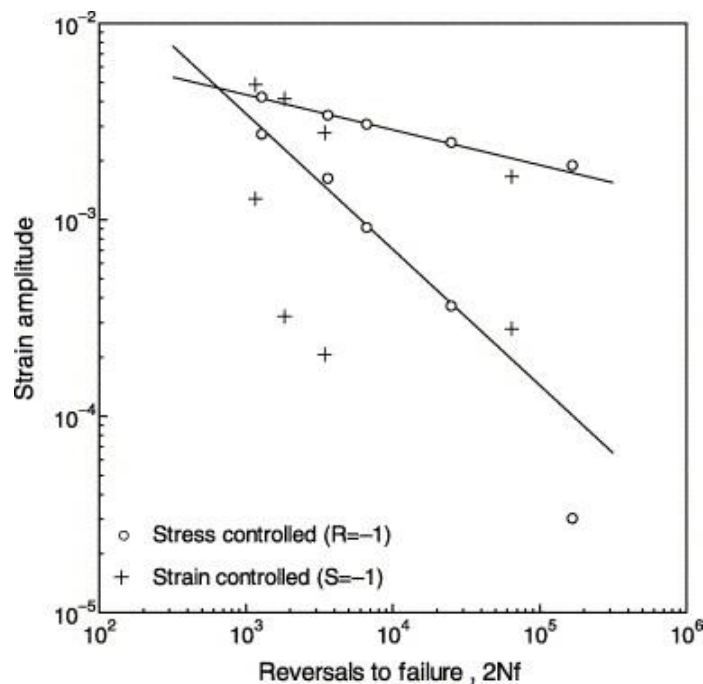


**Figure 2–3: Coffin-Manson model of AZ31B [19]**

A very high cycle experiment has been performed by Yang et al. and the reported $88.7\pm4.1$ MPa in run out of $10^9$ cycles for extrude samples [21]. Figure 2–4 shows the S-N curve of their experiments. A low cycle regime and a comparison of the strain-based and stress-based fatigue models of AZ31B extrude has been presented by Begum et al. [22]. Their results are shown in Figure 2–5. The influence of the direction of rolling in AZ31B rolled alloy has also been demonstrated by Park et al. [23], as well the fatigue limit of AZ31B.
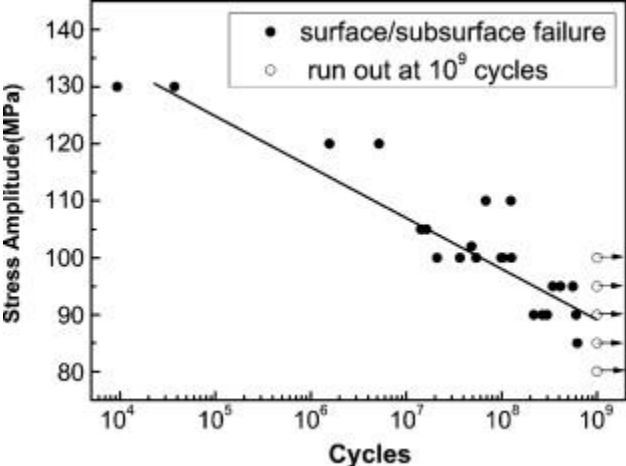


Figure 2–4: S-N curve of AZ31B [21]
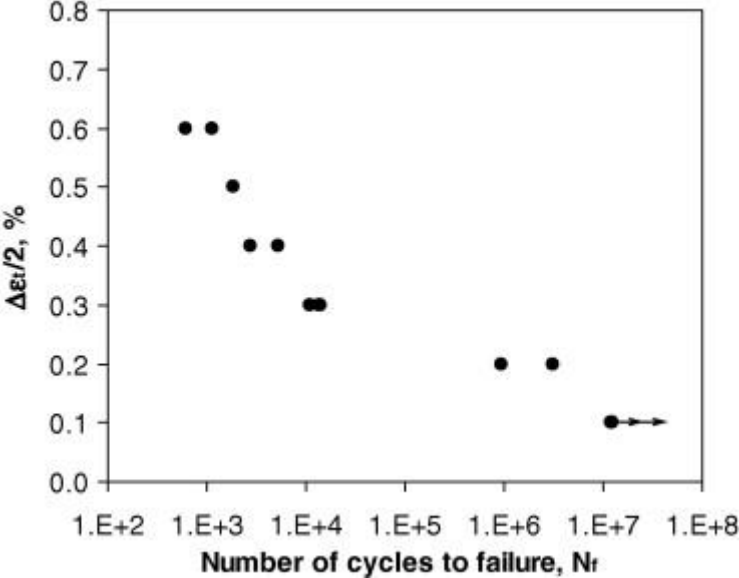


Figure 2–5: Strain-Cycle curve of AZ31B [22]

As presented above, there are relatively few studies on the fatigue behaviour of AZ31B cast alloy. A new fatigue test on this type of magnesium alloy is required to determine the fatigue limit of the alloy and to compare it with the improved fatigue limit after cold spray coating and top coating. In this research, the fatigue limit of AZ31B cast alloy samples has been studied using the stress-based method.

## 2.4 Cold spray mechanism

A method of coating using high velocity deposition of coating material particles was patented by Rocheville in 1963 [24]. This idea was followed and tested experimentally at the Institute of Theoretical and Applied Mechanics of the Siberian Branch of the Russian Academy of Science (ITAM of RAS) in the 1980s [25]. Briefly, the cold spray process works based on cohesion of the coating material particles on the surface of the substrate, delivered at high speed through a nozzle via a carrier gas. Figure 2–6 presents a schematic view of cold spray deposition [25].
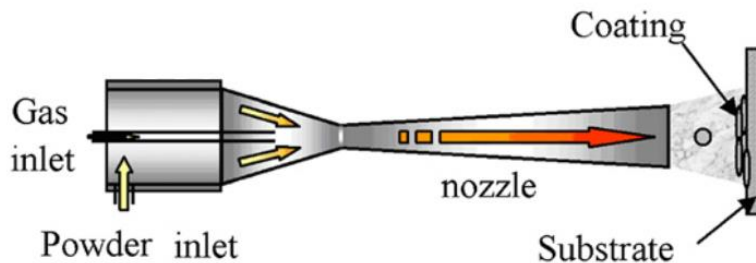


**Figure 2–6: Schematic view of cold spray deposition and cohesion of the particles on substrate surface [25]**

Measurement of the velocity of the particles is very difficult, but modeling and calculation of the conditions have been performed and particle velocity has been extracted by various researchers. This velocity varies depending on the density, pressure, and temperature of the carrier gas, nozzle profile, particle shape and size, and density. The velocity for common materials used as coating is between 300 and 1200 m/s.

The mechanism of adhesion between the coat and the substrate continues to be studied, and most research that has been done demonstrates that it is not well understood [24], [26], and [27]. However, it has been simulated and simplified by an analogy to adhesion of a mud ball on a wall after impact. A study has been performed in detail for modeling the impact in the cold spray process and the phenomenon has been referred to as shear instability during the very short period of the impact [26]. This shear instability causes an increase in temperature of the particles and may induce localized melting of particles. This local melting causes adhesion of the particles to the substrate surface. Figure 2–7 shows different steps of the particle impact during the cold spray deposition process.
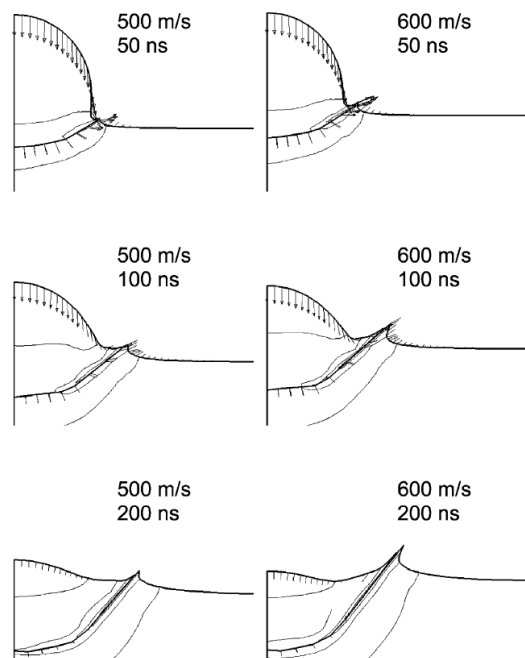


**Figure 2–7: Modeled impact of a particle to a substrate surface at different time steps [26]**

Variations in the stress, strain, and temperature have also been simulated by the model presented by Assadi et al. [26]; these are presented in Figure 2–8.
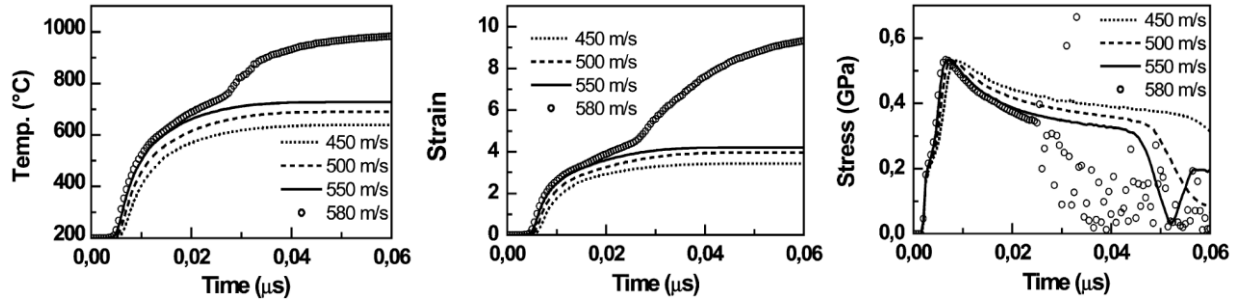
**Figure 2–8: Variations in temperature, strain, and stress (from left to right) of a particle during impact in cold spray [26]**

In this research, we are interested in the effect of cold spray process on the substrate. This process has different applications such as manufacturing method, part repairmen, surface covering etc.

A by-product of cold spray process is formation of residual stresses. Residual stress caused by the cold spray has been examined in some studies. Figure 2-9 shows a schematic of particle collision with the substrate in cold spray, leading to formation of beneficial residual stress. Typical residual stress distribution at and near the surface is also shown [4]. Among different effect of this process, the residual stress that remains on the substrate and coat after the cold spray process, leads to use the process for improvement in fatigue resistance because compressive residual stress leads to enhancement of the fatigue limit and causes delay in crack during cyclic loading [28]
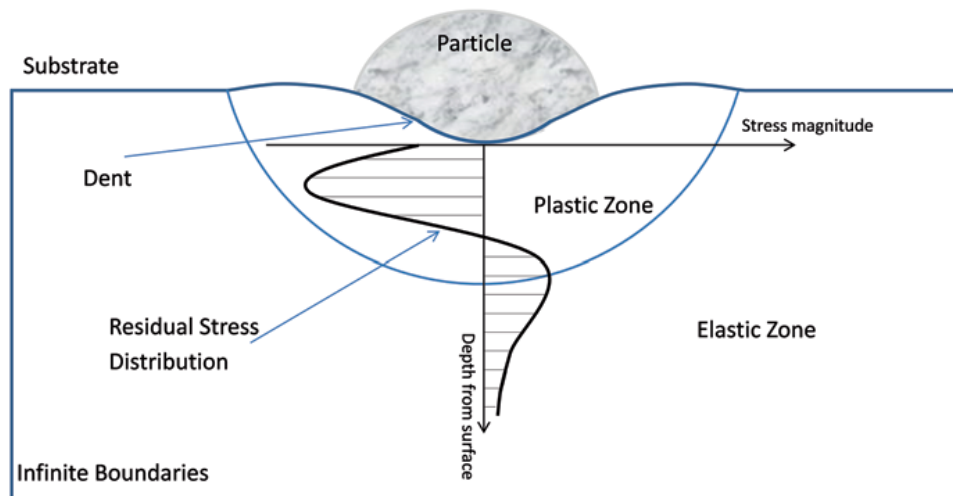


**Figure 2–9: Schematic view of particle impact and stress induced in the coat and the substrate [4]**

As reviewed above, this compressive residual stress will have a positive effect on fatigue resistance of the substrate, which is a magnesium alloy of AZ31B. Other than the effect of residual stress, the existence of a work-hardened layer, which carries a part of the stresses in cyclic loading leads to improved fatigue resistance of the material.

## 2.5 Cold spray on magnesium alloys

Cold spray on magnesium alloys has been performed for different reasons such as corrosion improvement, surface properties improvement, and fatigue resistance improvement. DeForce et al. [29] performed cold spray of pure aluminum on ZE41A magnesium alloy and investigated corrosion behaviour of coated samples. They reported improvement of corrosion resistance of coated samples. Reasons of this improvement were reported as surface covering and corrosion protection of the substrate. Bu et al. [30] performed cold spray of three different percentages of aluminum and $Mg_{17}Al_{12}$ on AZ91D substrate to investigate corrosion behaviour of coated and uncoated samples. They reported improvement of the corrosion resistance of coated samples. Spencer et al. [31] performed cold spray in three different percentages of alumina and Al 6061 powder on AZ91 magnesium substrate. They reported increase of surface hardness and corrosion resistance of coated samples. Their results showed that the coating material that had higher hardness also had higher bonding strength. To increase the fatigue resistance of the substrate Fu et al. [32] performed spray coating of a chromium composition on titanium alloy and they demonstrated improvement in fatigue resistance of the substrate after coating. They reported compressive residual stress as the reason of fatigue resistance improvement. Another related study was performed by Lee et al. in 2013 [33], in which two coating materials: IN625 and 301 stainless steel, were cold spray deposited on AZ80 magnesium alloy. Figure 2–10 shows the cross-section of the coat and hardness distribution of IN625

coating on AZ80. The authors demonstrated that by applying the cyclic potentio-dynamic polarization method and 24 hr salt spray test, both IN625 and SUS301 coating prominently enhanced the corrosion resistance of AZ80 magnesium alloy substrate. Further study is required to determine the effect of the process on fatigue properties of this magnesium alloy.
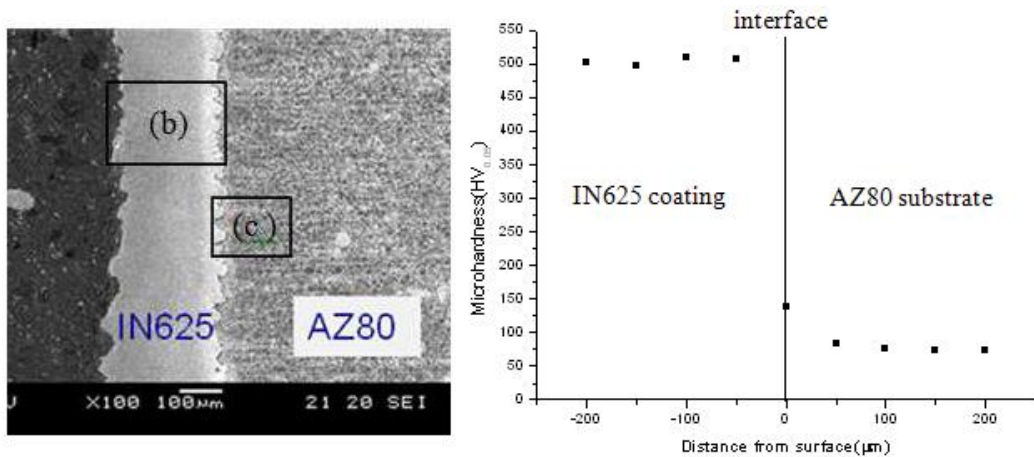


**Figure 2–10: Cross-section of the coat (left) and hardness distribution of coating of IN625 on AZ80 [34]**

Among the different methods of enhancing fatigue resistance, some are focused on cold work hardening and preparation of residual compressive stress, which is related to this research. Cold spray of an aluminum alloy as a multipurpose method of coating was selected for improving the fatigue limit of AZ31B cast alloy for this study.

The effect of cold spray deposition on inducing compressive residual stress has been studied [34], [4], and [35]. Research on two types of coating material showed different effects on fatigue resistance: an improvement in fatigue resistance was observed for Al 7075 on Al 5052, and a reduction in resistance for titanium on Ti6Al4V in comparison to un-coated materials [4]. In general, the compressive residual stress is able to increase the fatigue resistance of a material by preventing delamination of the material's grains [35]. Pure aluminum as a coating has been performed by Kalatehmollaei et al. [36] in cold spray deposition on AZ31B extruded alloy, and researchers observed a 9 % increase in fatigue resistance. Compressive residual stress in

16

coating and interface region of the substrate has been reported as the reason of this improvement. Another study attempted to perform deposition of aluminum AZ91D magnesium alloys, and the results demonstrated acceptable bonding strength [30]. Diab et al. [37] followed the cold spray of pure aluminum on AZ31B extrude alloy to investigate corrosion-fatigue resistance of coated samples. They report lower corrosion-fatigue resistance of coated samples in comparison to un-coated samples. The reasons of this phenomenon were known as the higher crevice corrosion on coated samples under the coat regions and sacrificing the substrate to the coat caused by higher galvanic tendency of magnesium than aluminum. According to the positive effect of the hardness of the coat reported in [31] and the stronger fatigue properties of Al 7075 coated samples reported in [38], coating material selected for this study is Al 7075 powder, and the coating process selected was a low pressure cold spray system For prevention of the corrosion another top coating has been applied which will be studied in chapter five.

## 2.6 Cold spray of Al 7075 as coating powder

Based on the finding of the studies described above, a stronger aluminum alloy has been chosen as the coating material for AZ31B for this study. Among aluminum alloys, Al 7075 is demonstrated to have the highest fatigue resistance, according to test results [39]. The stronger mechanical properties of Al 7075, in comparison to the strength of other aluminum alloys, leads to lower deposition efficiency of this material in cold spray deposition and lower usage in cold spray coating. To date, cold spray deposition of Al 7075 on a magnesium alloy, has not been reported in the open scientific literature. However, because of the acceptable strength of the coating, Al 7075 has been tried on other substrates than Mg. Ghelichi et al. [38] demonstrated a comparison of the fatigue strength of Al 5052 substrate with two different coating materials: pure aluminum and Al 7075. They achieved a greater improvement in the fatigue limit of the

substrate with the Al 7075 coat, in comparison to the pure aluminum coat. Figure 2–11 shows SEM images of the fracture surface of coated samples with pure aluminum and Al 7075 on Al 5052 substrate.
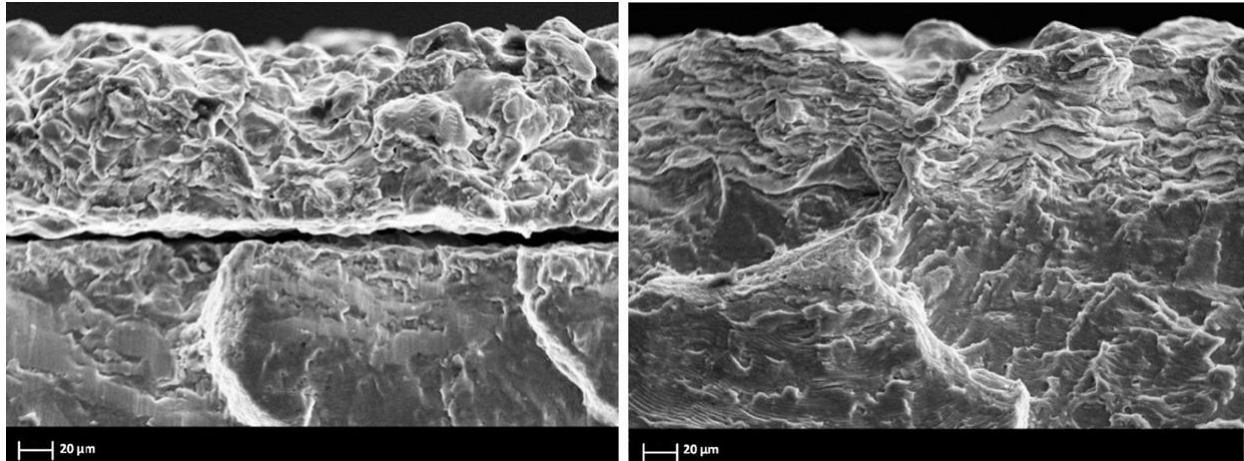


**Figure 2–11: Fracture surface of coated samples with pure aluminum (left) and Al 7075 (right) on Al 5052 [38]**

In this study, they achieved a 20 % improvement in fatigue limit and a 10 % improvement in regime line. Table 2-4 represents the S-N curve of two types of coating. Comparison of the influence of coating material has been shown in Figure 2–12

**Table 2-4: Fatigue strength of different series of specimens [38]**

| Sample condition | Fatigue limit (MPa) | S-N curve (equation of the line) |
|---|---|---|
| Al 5052 as received | 96 | -30.7 log N + 295.4 |
| Al 5052 grit blasted | 108 | -30.7 log N + 316.5 |
| Al 5052 coated with pure aluminum | 104 | -21.6 log N + 244.2 |
| Al 5052 grit blasted coated wit pure aluminum | 108 | -19.9 log N + 237.9 |
| Al 5052 coated with AL 7075 | 123 | -21.8  log N + 264.4 |
| Al 5052 grit blasted coated with Al 7075 | 126 | -22.3  log N + 273 |
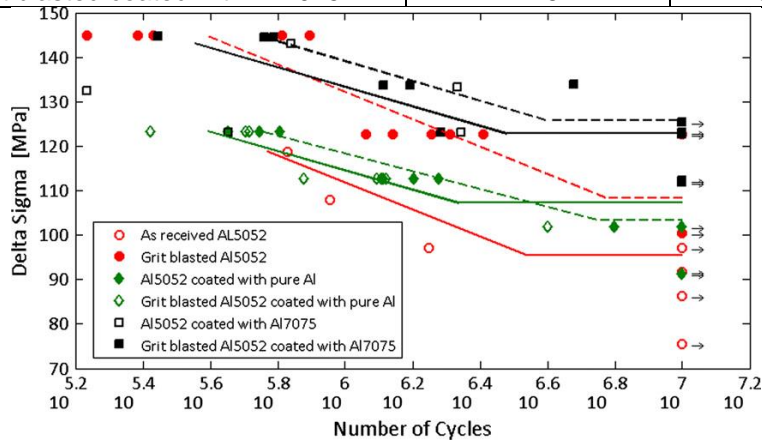


**Figure 2–12: Fatigue limit (MPa) of Al 5052 coated by pure aluminium and Al 7075 [38]**

18

Another study that used Al 7075 as coating material was performed by Rokni et al., in which Al 7075 was deposited on Al 7075 by a high pressure cold spray system with helium as the carrier gas [40] and [41]. The strength of the coat has been tested by two types of the strength tests: the shear lug test and the tension test. The tests confirmed the occurrence of strong cohesion and adhesion forces (as discussed in chapter 3) between the coat, and between the coat and the substrate, respectively [41]. In this study, the fatigue property and the effect of cold spray on it were not evaluated, however a strong bonding force and the ability of the Al 7075 coating were presented; these factors have led this material as coating powder in the present research, which will be discussed further in the next chapters.

# Chapter 3  Cold spray system and experiments

## 3.1 Facilities of the cold spray system

The system used for coating depositions is a low-pressure cold spray system manufactured by Centerline Co. Windsor, Ontario. The model is SST series P, and its units are described in Table 3-1.

**Table 3-1: The units of the cold spray system used to perform the coatings**

| Main cabinet | Dust collector | Pressure unit | Powder feeder | Power unit and control panel | Movement robot and software |
|---|---|---|---|---|---|
| Centerline Co. | W-3000 Diversi-tech Inc. | SST series P, Centerline Co. | AT-1200 Termach Inc. | Centerline Co. | ERC3 Inteligent Actuator Co. |
|  |  |  |  |  |  |

The system has a cabinet in which all the cold spray processes are performed in this cabinet. Two types of coatings are available with this system. First, for fixed flat samples, coating is applied by reciprocation movement of the nozzle; this method requires that the entire region of the substrate be swept. Second, coating on cylindrical samples is performed by longitudinal movement of the nozzle, while the sample is rotated by the chuck holder. The geometrical limits for the flat samples depends to the movement of the robot, and is approximately 75 cm in length and 20 cm in width. For the cylindrical samples, the limits depend on the chuck holder size; with the regular chuck holder, the limit is up to 20 mm in diameter. The available range of the linear speed of the nozzle movement, known as traverse speed, is 0.5 mm/s to 50 mm/s. The rotation speed of the chuck varies from 0 – 40 rpm.

There are different types of nozzles that can be connected to the system, but the nozzle holder needs to have an outer diameter of 8 mm. However, other sizes of nozzle can be connected by using the other nozzle holder. The system is compatible with the common types of the nozzles of different materials. According to the suggestion of the manufacturer [42] the nozzle used in these trials was a steel de laval nozzle, with the commercial name, UltiLife nozzle. The dimensions of the nozzle are presented in Table 3-2.

**Table 3-2: The properties of the nozzle used in the coating deposition process**

| Length | Orifice diameter | Exit diameter | Profile type | Material |
|--------|------------------|---------------|--------------|----------|
| 120 mm | 2 mm | 6.3 mm | De Laval [42], [24] | High strength stainless steel |

The system is a low pressure system with maximum available pressure and temperatures of 250 psi (1.72 MPa) and 550 $^0$C respectively; the trials were performed at pressures and temperature below these limits. The other parameters of the coating deposition process were also selected with consideration of the suggestions of other

researches, reviewed in Chapter Two, or based on the limits or availability of the sources. The basis for the selection of other parameters is explained below.

## 3.2 Coating parameter selection

3-2-1 Carrier gas: For such experiments, the carrier gases typically recommended are air, helium, nitrogen, or a mixture of these gases in different proportions [24]. Figure 3–1 shows the deposition efficiency of cold spray process by two different carrier gases.
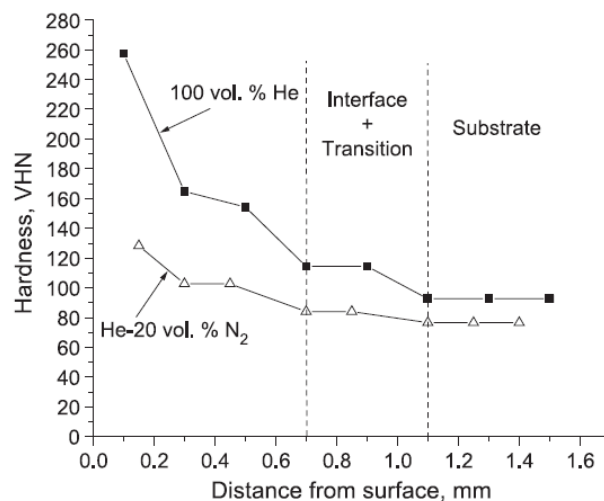


**Figure 3–1: Comparison of the effect of carrier gas versus coating hardness (Al 1100 on Al 1100) [44]**

Of these carrier gas options, nitrogen, helium, and air were available for the system. Air was not selected because of low coating performance [25], and helium was not selected because of the potential for leakage, the high cost, and difficulty of supply. Nitrogen tanks prepared by Praxair Co. were used.

3-2-2 Gas pressure: Two important parameters, pressure and temperature, play key roles in the velocity of the particles in the cold spray coating process [25]. To reach the required range between critical velocity and erosion velocity, a defined set of parameters is required. However, because the coating material Al 7075 has higher hardness and lower deposition efficiency than other aluminium alloys, it is hard to reach the erosion velocity using a low pressure system. Maximum pressure supplied by

the system is 250 psi. Trials were performed within the pressure range of the system (50 psi to 250 psi), while the other parameters were unchanged, for Al 7075 powder on AZ31B flat samples. The results show that the higher pressure, the thicker coating on the substrate at a gas temperature of 400 $^0$C (Figure 3–**2**).
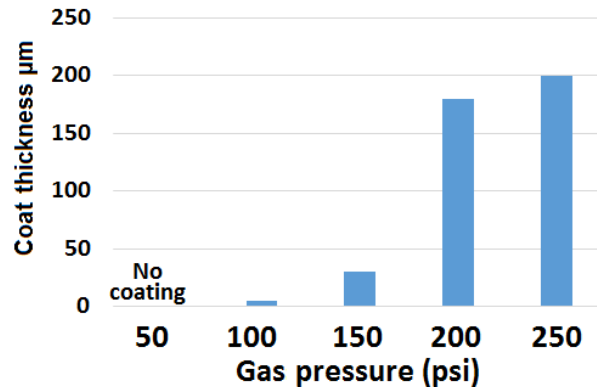


**Figure 3–2: The effect of gas pressure on coating thickness of (Al 7075 on AZ31B)**

This observation demonstrates to maximize the effect of the coating process, the highest available pressure is required. However, at high pressure operation, the temperature available for preheating the gas is limited; therefore the use of maximum pressure precludes the uses of high temperatures for continuous coating deposition. Thus, the pressure selected for the process was 200 psi.

3-2-3 Gas temperature: as explained in the previous section, system restrictions prevent reaching the erosion velocity. Some trials have been performed in the available range, and the results (Figure 3–**3**) demonstrate that a gas temperature of 400 $^0$C is optimal. The trials were performed at a gas pressure of 200 psi. A temperature of 400 $^0$C has been used in other researches as well [32], [31].
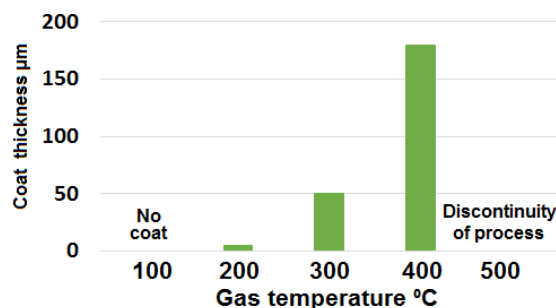


**Figure 3–3: The effect of gas temperature on coating thickness (Al 7075 on AZ31B)**

3-2-4 Feed rate: To select the feeder rate, an optimization has been performed. In most of the papers reviewed, the feed rate is not mentioned, however, one study indicated a powder feed rate of 60 gr/min [45].The experiments were performed at different feed rates and, as in the pressure and temperature trials, the target was coating thickness. Figure 3–4 represents the coating thickness at different feed rates. For these trials, all other parameters were constant (T: 400 $^0$C, P: 200 psi)
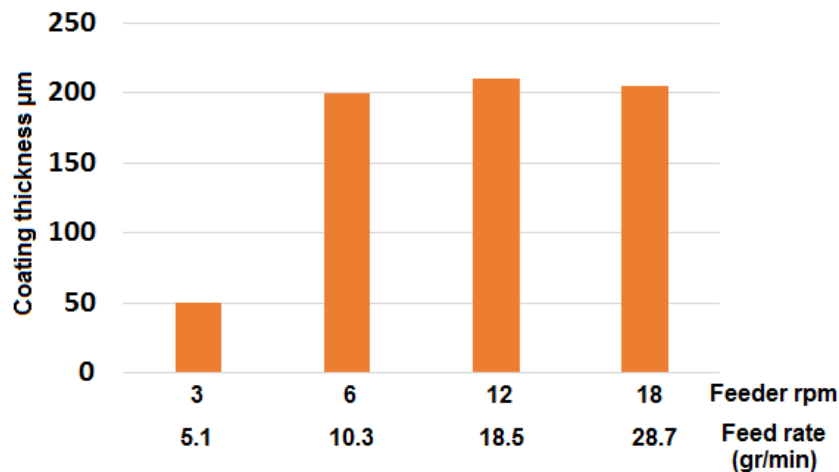


Figure 3–4: The effect of feed rate on the coating thickness (Al 7075 on AZ31B)

The cold spray system allows for the selection of a percentage value for feeding. Following the results of the optimization experiment, which shows that increasing the feed rate above 10 gr/min does not have a significant effect on the thickness, a feed rate of approximately 10 gr/min was selected; this is 25 % of the feed rate setting of the system, and translates to a feeder rotation speed of 5.23 rpm. Figure 3–5 shows the system panel with these parameters.
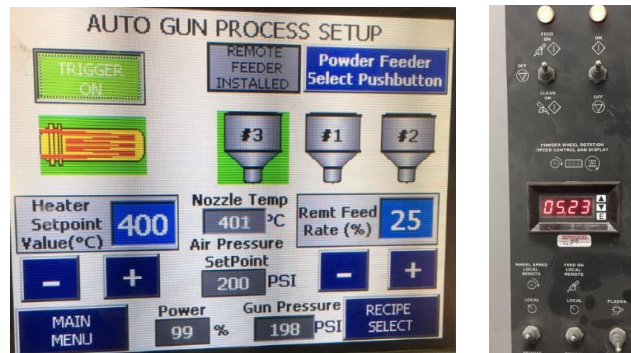


Figure 3–5: The panel of the system showing selected parameters (left) and the feeder rpm (right)

3-2-5 Stand-off and step-over distance: The system allows for the distance between the nozzle and the surface of the substrate to be set anywhere from 5 to 20 mm [25]. The recommendation of the system manufacturer [46], a distance of 12 mm has been selected for all trials. The step-over distance is the distance between each pass of coating to the previous and next pass. This parameter also varies and depends on the stand-off distance, nozzle shape, and required thickness. The system manufacturer's recommended a value of 1.2 mm of step-over. The stand-off distance and adjustment of the vertical position of the nozzle setting, is shown in Figure 3–6.



**Figure 3–6: The adjustment of the nozzle vertical position (left) and the stand-off distance (right)**

The step-over distance is also adjustable as well in the programming of the robot movement or in the setting of the rotating chuck, depending on where the substrate is flat or round.

3-2-6: Traverse speed: The final parameter, which has an important role on the coating thickness is the traverse velocity of the nozzle. Obviously, the lower the traverse speed, the thicker the coating on the substrate, but the amount selected depends on the required thickness. The trials displayed in Figure 3–2, Figure 3–3, and Figure 3–4 were performed at a traverse speed of 2 mm/s.

## 3.3 Coating material

3-3-1 Coating material selection: As reviewed in Chapter Two, the effect of cold spray deposition on inducing compressive residual stress was studied [4]. Based on the findings described in previous chapter, a stronger aluminium alloy is the most suitable candidate for coating material on AZ31B for this research. Al 7075 has been selected.

The coating material Al 7075 has been selected, and the coating process has been performed by a low pressure cold spray system. The characterization of the coat and performance tests have been conducted to evaluate the effect of the process and to make the process comparable to other research on improving fatigue resistance of magnesium alloys and determining the propagation of the crack and failure criteria.

3-3-2 Coating material characterization: According to the research described above, the Al 7075 coating powder (purchased from SST Centerline Co.) was used. The coat has been characterized using two approaches: chemical analysis of the powder, and size morphology of the particles. Figure 3–7**Error! Reference source not found.** presents a SEM image of an Al 7075 particle prepared with the WATlab SEM at the University of Waterloo.
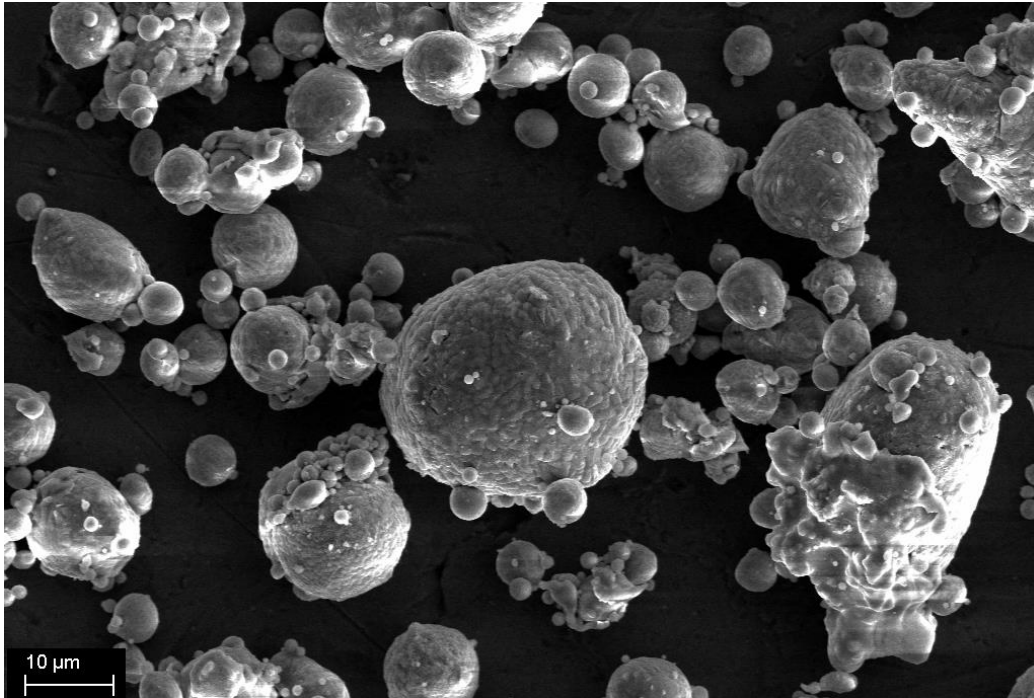
**Figure 3–7SEM image of the Al 7075 powder used as coating material**

The geometrical properties of the particle described by different parameters such as aspect ratio, shape factor, and circularity [47]. Of these parameters, shape factor has been selected by some researchers for cold spray evaluation [48]. Shape factor, which is the ratio of the shortest diameter to the longest diameter, has been measured for 150 particles in 5 different SEM images; the results are presented in Table 3-3.

**Table 3-3: The results of shape factor measurement of the Al 7075 powder particles**

| Shape factor | Confidence interval |
|--------------|---------------------|
| 0.827 ± 0.082 | 95 % |

The other geometrical characterization performed was particle size distribution; the results are presented in a histogram (Figure 3–8). Size distribution data was obtained through measurements of the particle diameters in the SEM images. The measurement was performed manually, and by counting the particles in each size group. The particles are categorized into different size groups, and the histogram bars represents the percentage of particles occurring in each group.
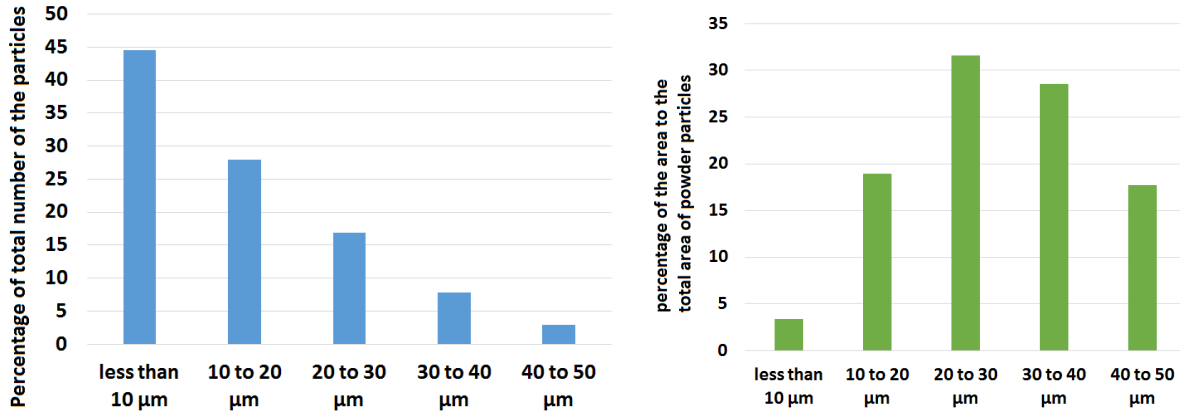
**Figure 3–8: the results of size measurement of the powder particles by SEM images of the powder percentage of particles number in each groups (left) , area percentage of the particles in each group (right)**

Chemical composition of the powder was performed by EDX of the SEM imaging in WATLab at the University of Waterloo. The measurement was repeated for three different samples, and the results are presented in Table 3-4.

**Table 3-4: Chemical composition of the coating powder Al 7075**

| Element | Weight % |
|---|---|
| Zinc | 5.2 |
| Magnesium | 2.35 |
| Copper | 1.55 |
| Iron | 0.35 |
| Chromium | 0.25 |
| Aluminum | 90 |
| Other elements | 0.3 |

## 3.4 Substrate of AZ31B

As explained in the introduction (Chapter One), the substrate that is under study is AZ31B cast alloy. The samples are prepared from 30 cm diameter billets in two shapes: flat samples and round samples. The chemical composition analysis was also performed for the substrate alloy by EDX of SEM in WATLab at the University of Waterloo. Table 3-5 shows the results.

**Table 3-5: Chemical composition of the magnesium cast alloy**

| Element | Weight % |
|---|---|
| Magnesium | 95 |
| Aluminum | 3.29 |

| Zinc | 1.33 |
|---|---|
| Manganese | 0.37 |

There are certain substrate specifications that play an important role in fatigue resistance of the material, which is explained further in Chapter Four. One of them is the porosity of the cast material, which can cause crack initiation. SEM images of the fracture surfaces will be discussed in Chapter Four.

## 3.5 Coating deposition and characterization

Characterization of the coat and substrate material, and selection of the process parameters led to the performance of some trials to identify acceptable coating quality. This process was performed successfully for flat samples, and after the parameters were finalized, was applied to round samples. The finalized parameters are presented in Table 3-6.

Table 3-6: The finalized parameters in the coating depositions

| Carrier Gas | Nitrogen |
|---|---|
| Gas Pressure | 1.4 MPa (200 psi) |
| Gas Temperature | 400 °C |
| Feeder rate | 5 rpm (8 gr/min) |
| Travers Velocity | 2 mm/s |
| Step over | 1.2 mm |
| Stand-off distance | 12 mm |
| Nozzle Type | De Laval UltiLife TM |
| Nozzle Length | 120 mm |
| Nozzle orifice  diameter | 2 mm |
| Nozzle exit diameter | 6.3 mm |

3-5-1 Porosity measurement

Porosity measurement was performed by cross section preparation and imaging of the coated samples. Visual evaluation was conducted by optical microscope and for higher quality, imaging was performed by SEM. The porosity was calculated as the ratio of the area of hollowed regions to the total area of the region as determined by measurement of the SEM images. Figure 3-9 shows an example of the detail of this measurement.
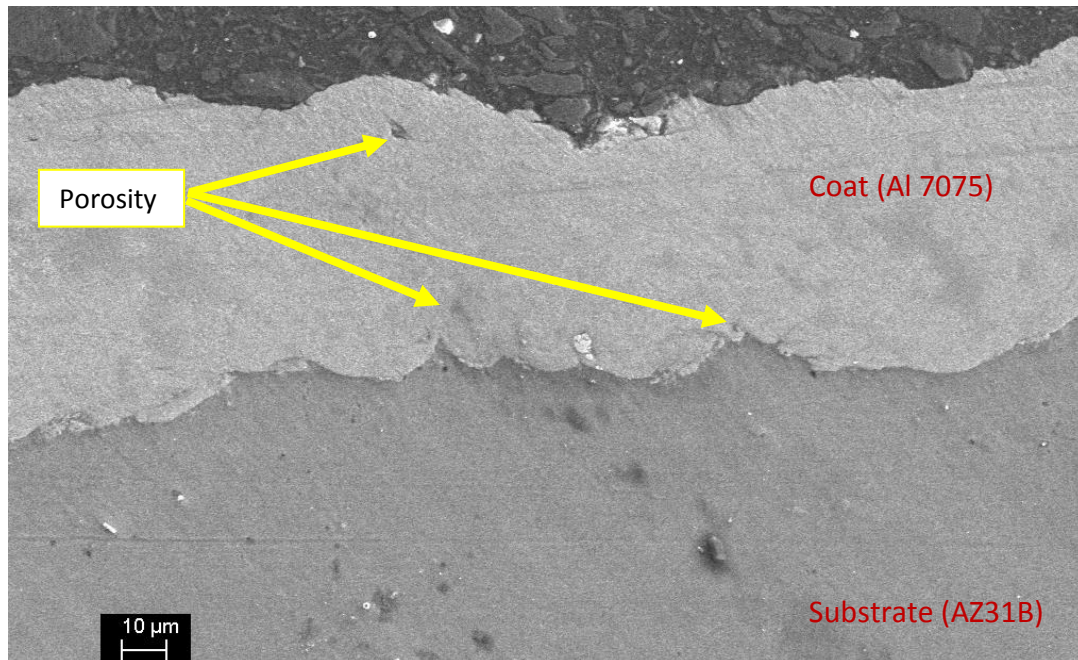
**Figure 3–9: SEM image of the cross section of a cold spray coated sample**

As explained above, the porosity was determined for five different SEM images as the ratio of the porosity area to the total area of the coat in the cross sections. This value measured was 4 %, which is an acceptable low-porosity coat in comparison to other cold spray coating on magnesium alloys [49].

3-5-2 Hardness test

The hardness test was performed by a micro-hardness Vickers test device (Model 402 MVD) in the Material Laboratory at the University of Waterloo. The measurement conditions were those indicated by ASTM E384-99: room temperature with an indentation force of 10 Ns in 15 seconds. Figure 3–10 represents the optical microscope image of the indent after the hardness test and Figure 3–11 shows the results of the hardness test.
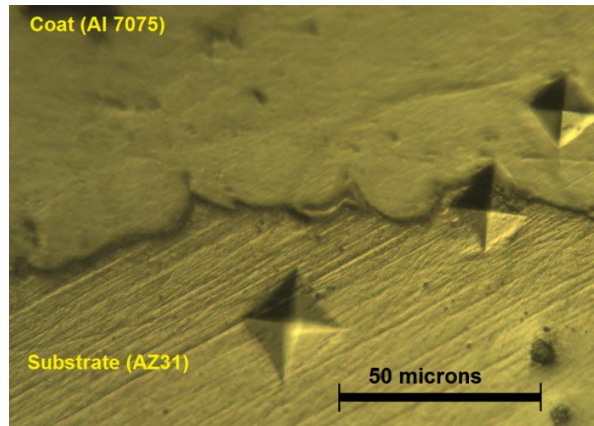
**Figure 3–10: Optical microscope image of the coat and substrate measurement of hardness**
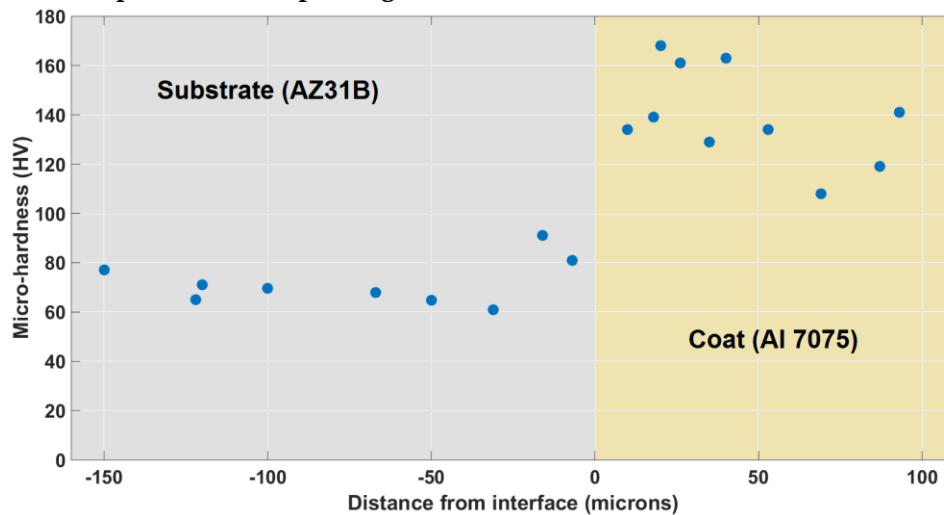


**Figure 3–11: Hardness distribution of the substrate and the coat vs the distance from interface**

A comparison between the hardness of the coated sample in this study and that reported in a study that used Al 7075 as the cold spray coat is presented in Table 3-7

**Table 3-7: Hardness of Al 7075 coat in the current research and what performed in** [42]

|  | **Micro hardness** |
|---|---|
| **Hardness of the coating Al 7075 on AZ31B** | 139.6 ± 19.4 HV |
| **Hardness of Al 7075 coating on Al 7075 [40]** | 115 ± 9 MPa (as sprayed) 162 ± 3 (after heat treatment) |

3-5-3 Tension test

Some methods have been developed to evaluate the general quality and bonding strength of the coat. These methods enable the measurement of the maximum strength of the bonding force between the coat and the substrate, or known as the coat cohesion

force. Some of the common methods for evaluating cold spray quality include Tension tests for measuring the tension strength of the coat, according to the methods of ASTM C633 or EN 582; a shear lug test according to the methods [49], [50] for measuring the shear strength of the bonding force; and a tabular test method to measure the cohesion force of the coat. Figure 3–12, Figure 3–13, and Figure 3–14 depict the lug shear test, tabular coating tensile test, and tension adhesion test, respectively.
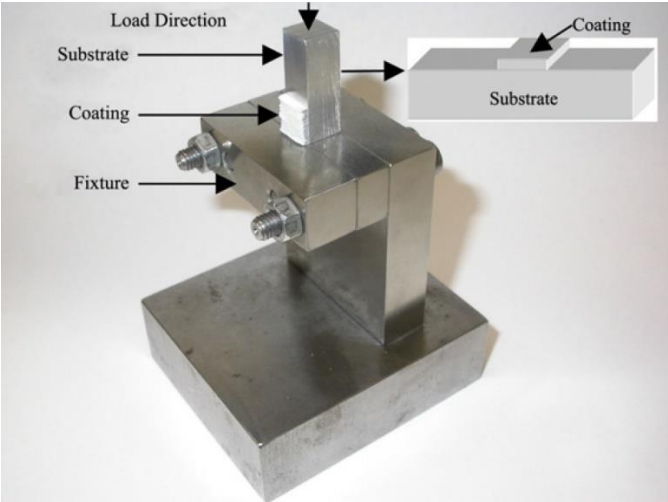


**Figure 3–12: Lug shear test [50]**
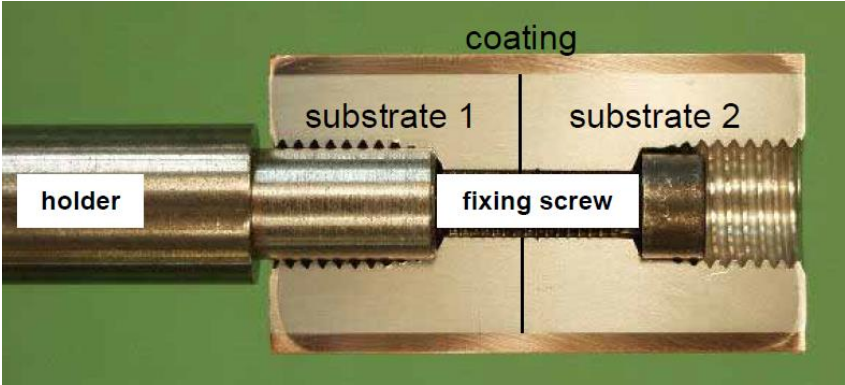


**Figure 3–13: Tabular Coating Tensile Test (TCT-Test) [51]**
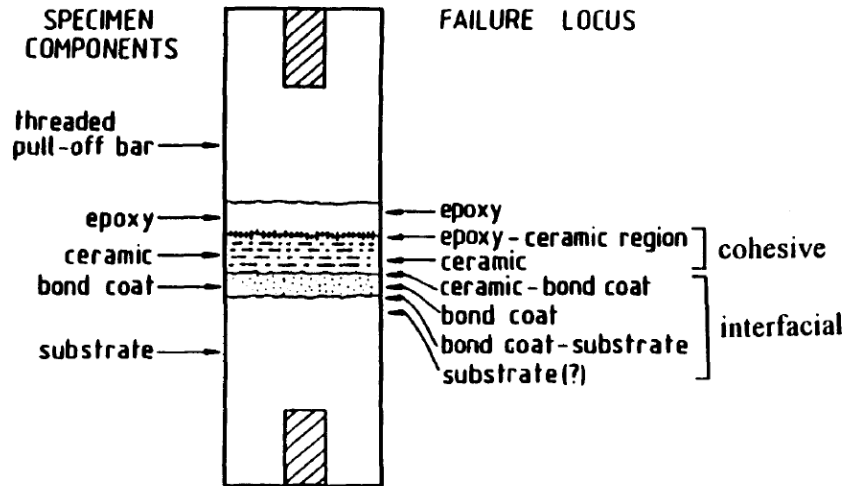
**Figure 3–14 Tension adhesion test according ASTM-C633 [52]**

In this research, the tension adhesion test was performed according to methods of ASTM C633. Three coated samples were prepared using the final parameters indicated above (Table 3-8) on flat end of a cylindrical substrates of AZ31B with standard dimensions. The test was performed at Centerline Co, Windsor, Ontario. The substrate fixtures from AZ31B coated by Al 7075 were adhered to the loading fixture from steel by a commercially available M3 adhesive. Figure 3–15 shows the coated sample and the glued samples before tension testing. The results are presented in Table 3-8.
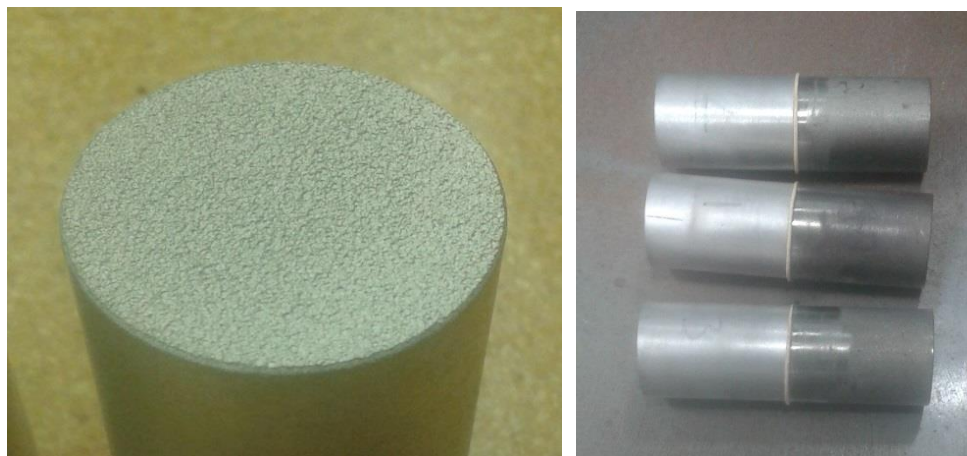


**Figure 3–15: The coated substrate fixture (left) and three prepared samples for tension test (right)**

**Table 3-8: The result of the tension test of Al7075 on AZ31B**

| Strength | $42.1 \pm 3.2$ MPa |
|---|---|
| **Failure mode** | Adhesion |

Failure mode represents the weakest strength among adhesion bond of the coat to the substrate, cohesion through the coat, or epoxy glue to the coat. Figure **3–16** represent the surface of the substrate after tension testing, and a schematic explanation of the failure types. The separation of the coat from the substrate is observable. Table **3-9** shows the results of some tension tests from other studies with methods similar to those performed in this study. The comparison shows acceptable results for the coating of Al 7075 on AZ31B cast alloy.
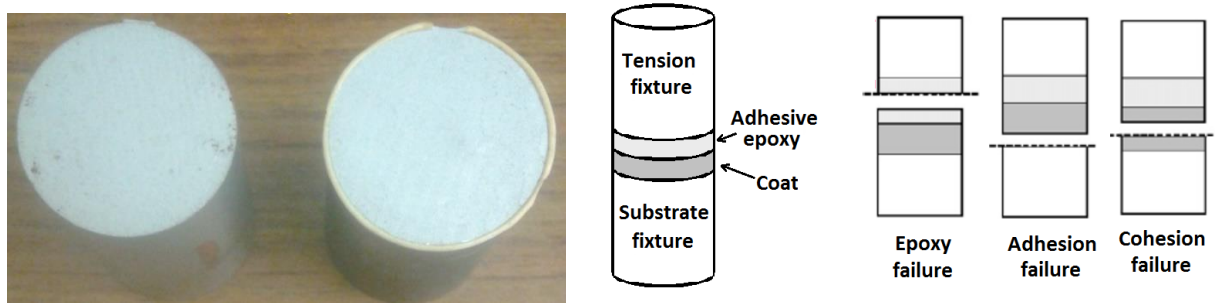


**Figure 3–16: Failed sample after tension test (left) and schematic of different failures (right)**

**Table 3-9: The result of tension test of Al7075 on AZ31B**

| Coating material on Substrate | Failure mode | Strength |
|---|---|---|
| Tungsten on Al 7075 [51] | Adhesion | 26 MPa |
| Al 6061 on ZE41 [53] | Adhesion | 76 MPa |
| WC-25Co on Al 7075 [54] | Adhesion | 74 MPa |
| Al-Alumina on AZ91 [30] | Cohesion | 40 MPa |
| Ni-Al on steel [55] | Adhesion | 50 MPa |
| Al 7075 on Al 7075 [39] | Cohesion | 83 MPa (after heat treatment) |
| Al on Al 7075 [49] | Adhesion | 40 MPa |
| Al 7075 on AZ31B (this research) | Adhesion | $42 \pm 3$ MPa |

3-5-3 Residual stress measurement

An important effect of coating deposition on the substrates is inducing residual stress, which is able to improve the fatigue resistance of the coated material. The residual stress measurement was performed on a flat sample of AZ31B by the methods of hole drilling and X-Ray Diffraction (XRD) by SINT technology (model: RESTAN) and BRUKER (model: D8 Discover), respectively. The results of stress measurement through the depth are presented in Figure 3–17. As well the result of measurement by XRD method is presented in Figure 3–18. It was observed that compressive residual stress, which plays a role in improving fatigue resistance, is present in the coating.
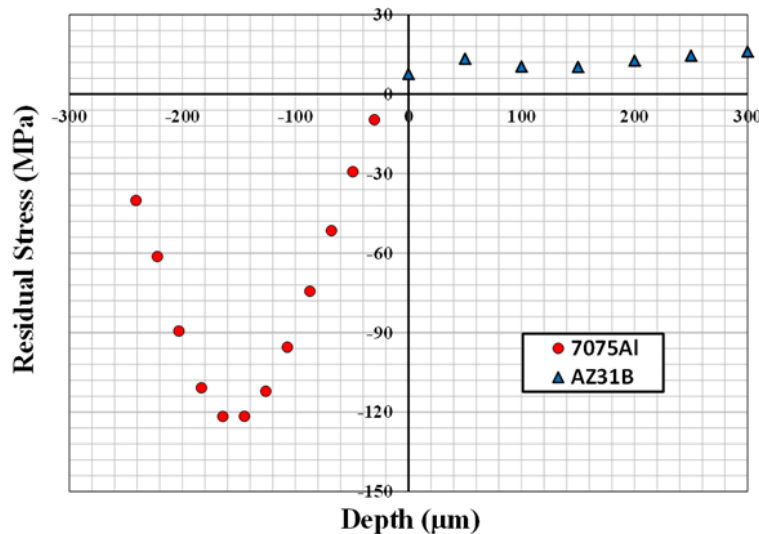


**Figure 3–17: Residual stress through the depth by hole drilling method, as a function of depth**
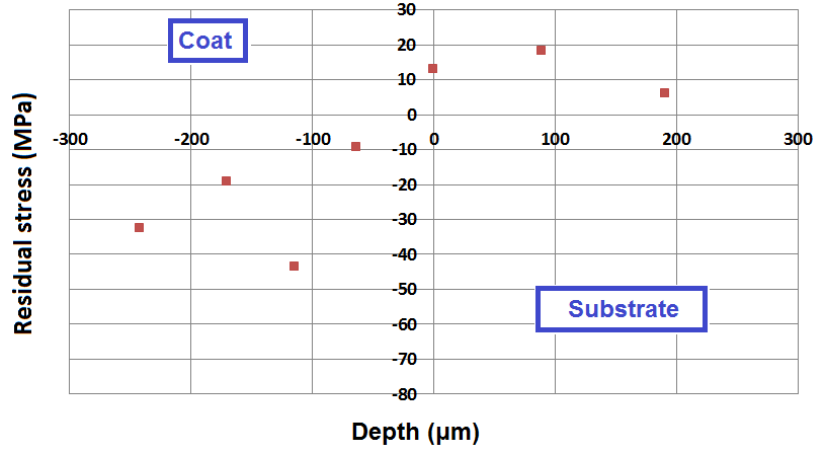
**Figure 3–18: Residual stress through the depth by XRD method, as a function of depth**

The tests and characterization described above verify the final acceptable coating processes and required parameters. Coating deposition on round samples was performed at the finalized parameters, and will be discussed in following two chapters.

# Chapter 4 The effect of cold spray on fatigue resistance

      Fatigue tests are performed according to different methods in different material labs. Two common methods available at the fatigue lab of the University of Waterloo are the uniaxial push-pull method and the rotating-bending method. The second method was selected for this research for two reasons. The first reason is to provide continuity with previous researches performed in this lab that has followed the rotating-bending method, and to enable the comparison of results between them. This method has been followed to perform the fatigue test of AZ31B samples coated by pure aluminium [36], [57] and corrosion-fatigue tests of AZ31B samples coated by pure aluminium [37]. The second reason is related to the effect of cold spray coating on the substrate, which occurs on the surface or close to the surface [4]. In rotating-bending tests, the maximum stress applied on the surface of the sample is based on the distribution of stress produced by the bending [58]. Figure 4–1 shows a schematic view of a four-point rotating-bending fatigue test device.
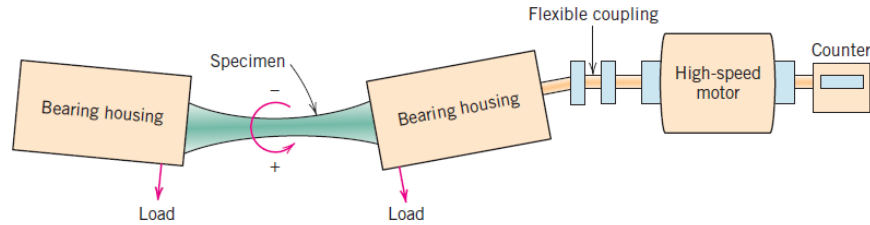
**Figure 4–1: Schematic view of a four-point rotating-bending fatigue test device [59]**

## 4.1 Sample preparation

The fatigue test device used in the performance tests of this research is Instron RR Moore. A drawing was prepared based on the size requirements and capabilities of the test machine (Figure 4–2); this drawing was used for the manufacture of about 120 samples in the engineering machine shop at the University of Waterloo.
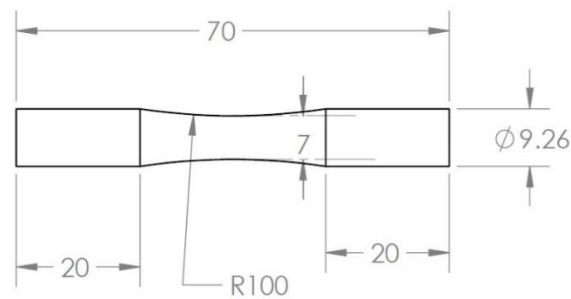


**Figure 4–2: Drawing of the samples**

An important part of the test requirement is the preparation of an acceptable uniform coat on the round samples. The required parameters and characterized coat were previously reached (discussed in detail in Chapter Three). However, the application of these parameters to the preparation of acceptable coats for round samples requires further trials and studies. Three types of coating on round samples are theoretically possible (Figure 4–3): parallel coating through the circumstance of the sample, circular coating through the length of the sample, and helical coating.
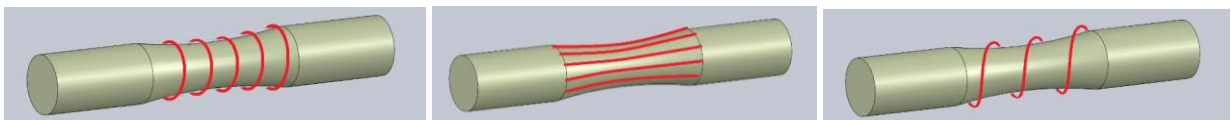


**Figure 4–3: Coating types on round samples: Circular (left), linear (middle), and helical (right)**

All of these methods can be performed with the cold spray system, but a method is required that is compatible with coating process parameters, especially the traverse velocity. As explained in the previous chapter, the final traverse speed of the nozzle gun on the substrate was 2 mm/s. To reach this traverse velocity in any of these three types of coating, the linear speed of the nozzle must be different from the rotational speed of the chuck holder. More details are presented in Table 4-1. The calculation was performed for a round sample with a radius of 3.5 mm.

Table 4-1: The required movement speed for different types of round sample coating

| Coating method | Rotation speed of collet chuck | Linear speed of the nozzle | Traverse velocity | Step-over |
|---|---|---|---|---|
| Circular | 5.5 rpm | Zero (in each pass) | $\frac{5.5 \times 2\pi}{60} \times 3.5\ mm = 2\frac{mm}{s}$ | 1.2 mm |
| Linear | Zero (in each pass) | 2 mm/s | 2 mm/s | $20^0 = \frac{20 \times \pi}{180} \times 3.5 mm$ $= 1.2\ mm$ |
| Helical | 40 rpm | 0.8 mm/s | $\sqrt{\left(\frac{40 \times 2\pi}{60}\right)^2 + 0.8^2} = 4.25\frac{mm}{s}$ | $= \frac{60}{40}s \times 0.8\frac{mm}{s}$ $= 1.2\ mm$ |

All the methods explained above are theoretically possible. However, under real conditions, there are some problems with applying the calculated parameters. For instance, the traverse velocity for helical coating is higher than what is required for linear coating (4.25 mm/s > 2 mm/s). Also, the increase in rotation speed required to reduce the traverse velocity leads to increased step-over. For example, a rotation speed of 17.5 rpm and nozzle speed of 0.8 mm/s are suitable; however, the resulting step-over exceeds 1.2 mm, as shown below:

Traverse velocity for 17.5 rpm (helical): $\sqrt{\left(\frac{17.5 \times 2\pi}{60}\right)^2 + 0.8^2} = 2\frac{mm}{s}$

Step-over for 17.5 rpm (helical): $\frac{60\ s}{17.5} \times 0.8\frac{mm}{s} = 2.75\ mm$

Based on the capabilities of the system and these calculations, the linear method has been selected for coating round samples. Figure 4–4 shows a sample before and after coating.



**Figure 4–4: Un-coated sample of AZ31B (top) and coated sample by cold spray of Al 7075 (below)**

The next stage of sample preparation is related to the roughness of the samples. To evaluate the effect of surface roughness on fatigue behaviour of the materials, surface roughness of bare samples was measured for fifteen samples, and the resulting Ra=0.65±0.15 μm for bare samples. This measurement was also performed for coated samples and it was considerable higher and out of range because of the rough surface of coated samples. All coated samples were polished to reach the same roughness as bare sample. Polishing was performed using sand paper # 320, 400, 600, and 1200, respectively. The surface roughness of coated samples after polishing was also measured for ten samples. The result (Ra=0.7±0.2μm) is almost the same as that for bare samples. The thickness of the coating for unpolished sample varies from 200 – 300 μm, and after polishing, the coating thickness was 100±10 μm. Figure 4–5 shows SEM images of coated samples before and after polishing.
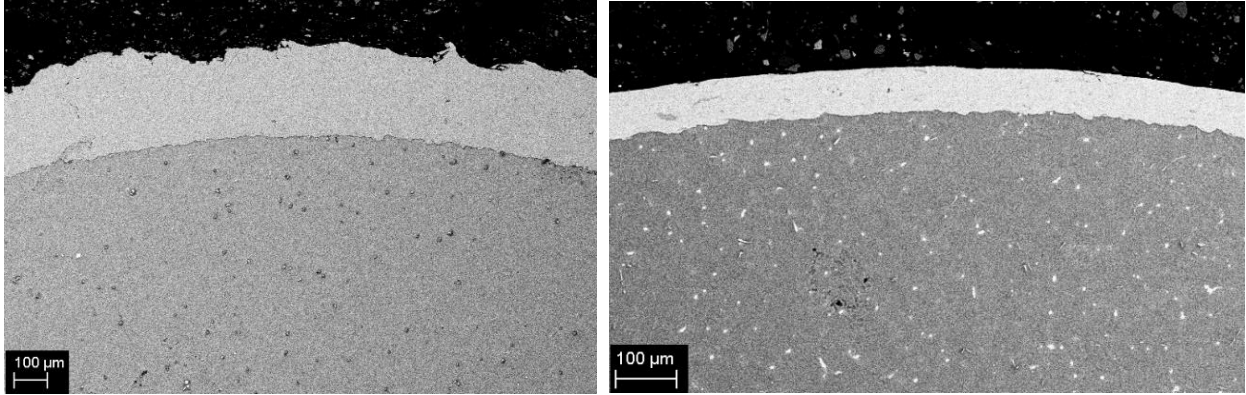
**Figure 4–5: SEM image of cross section of unpolished coated (left) and polished coated sample (right)**

## 4.2 Fatigue test device

As explained in previously, a four-point rotating-bending fatigue test machine was used for fatigue tests. Regarding the different factors that affect the amount of stress on the specimen, measurement of the actual value of the stress level is not possible, especially because of variation in the effective area of the sample during crack propagation. The method recommended in the manual of the fatigue device is load control stress measurement. This method was applied to all fatigue tests of this research. The equations below demonstrates the stress calculation for each load level. Figure 4–6 also shows a schematic view of the loading on specimen.
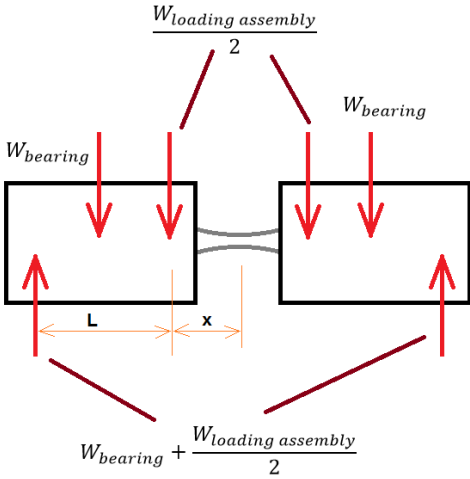


**Figure 4–6: Schematic view of loading on specimens in a fatigue test device**

41

$$\sum M = (W + \frac{W_{loading\ assembly}}{2}) \times (L + x) - W_{bearing} \times \left(\frac{L}{2} + x\right) - \frac{W_{loading\ assembly}}{2} \times x$$

$$= \left(\frac{W_{bearing} + W_{loading\ assembly}}{2}\right) \times L \Rightarrow W_{bearing} + W_{loading\ assembly} = W$$

$$\Rightarrow S = \frac{W\frac{L}{2} \times \frac{D}{2}}{\frac{\pi}{64}D^4} = \frac{16WL}{\pi D^3}$$

Using the equation above, the stress value was measured and controlled by the load value (W). Figure 4–7 shows the device. The other required value in the fatigue test is the number of cycles required to include sample failure. The cycles are counted during the rotation and are displayed on the machine. The frequency of the rotation does not have a significant effect on the results if the limits of the machine are not reached or stress heating of the specimen does not occur. Therefore, a frequency of 100 Hz was applied. Obviously the stress ratio in this condition is equal to -1. For all tests, ten million cycles is assumed to be the run-out limit. The "brief staircase" method presented by Dixon and Massey [60] was used to perform the tests with a stress step of 10 MPa, and the up and down method presented by Hodge–Rosenblatt [61] was used to calculate the fatigue strength corresponding to a fatigue life equivalent to the run-out limit. The fatigue test data was elaborated based on the ASTM standard E739-10 [62] to obtain the S–N diagram for different cases with a failure probability of 90 % on a bi-logarithmic scale.



**Figure 4–7: Rotating-bending fatigue test device [63]**

## 4.3 Fatigue test of bare samples

The fatigue test was performed on 18 bare samples over two weeks. The result obtained by decreasing the stress level to reach the run-out limit has been continued. After run-out, the sample up and down method was applied. Table 4-2 presents the results of the fatigue tests of bare samples.

Table 4-2: The results of fatigue test on bare samples

|  | Cycles | Stress | Result | Test duration |
|---|---|---|---|---|
| Different stress level from high stress to low stress | 4749 | 143 | Failure | ~ 1 minute |
|  | 5066 | 143 | Failure | ~ 1 minute |
|  | 14719 | 124 | Failure | ~ 2.5 minutes |
|  | 20496 | 123 | Failure | ~ 3.5 minutes |
|  | 68292 | 102 | Failure | ~ 11 minutes |
|  | 111240 | 103 | Failure | ~ 18.5 minutes |
|  | 124982 | 93 | Failure | ~ 21 minutes |
|  | 148720 | 93 | Failure | ~ 25 minutes |
|  | 1447452 | 93 | Failure | ~ 4 hours |
|  | 1954014 | 83 | Failure | ~ 5.4 hours |
|  | 2192255 | 83 | Failure | ~ 6 hours |
| Up and down of the stress level regarding to run out result | 10974802 | 63 | **No failure** | ~ 30 hours |
|  | 4948440 | 78 | Failure | ~ 14 hours |
|  | 10428766 | 70 | **No Failure** | ~ 29 hours |
|  | 5099116 | 78 | Failure | ~ 14 hours |
|  | 6166540 | 70 | Failure | ~ 17 hours |
|  | 10825085 | 76 | **No failure** | ~ 30 hours |
|  | 10013047 | 79 | **No failure** | ~ 28 hours |

Based on important information obtained from the fatigue test, the S-N curve of the test was extracted and is presented in Figure 4–8. The S-N curve was also extracted from all failed samples, and the average of up and down stress levels was measured as the fatigue limit of the material. The results of the regime line and fatigue limit are presented in Table 4-3.

Table 4-3: Regime line and fatigue limit of bare samples of AZ31B cast alloy

| Fatigue limit | $R^2$ | S-N curve |
|---|---|---|
| 73.4±5.9 MPa | 0.899 | $-22.075\, Log\, N\ + 218.82$ |
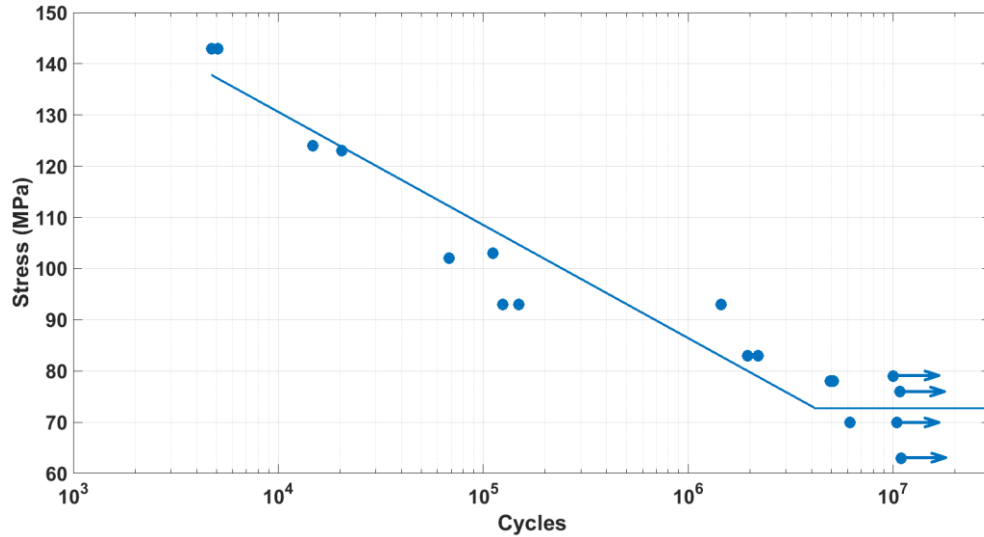
**Figure 4–8: S-N curve of fatigue test of bare samples of AZ31B cast alloy**

The fatigue limit of extruded AZ31B which was performed by Kalate,olaei [36] is higher than that of cast alloy. The reason for the lower fatigue limit of cast alloy can be investigated by examining the SEM images of the fracture surfaces. Figure 4–9 presents the SEM image of the fracture surface of a bare sample under 70 MPa of stress level and of 6 million cycles to fail.
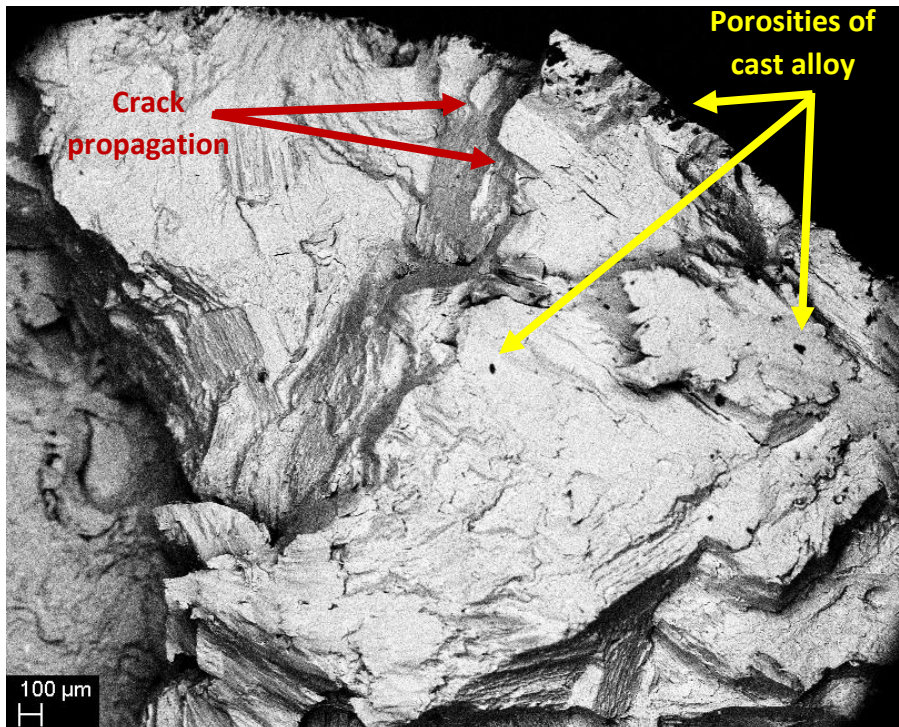


**Figure 4–9: SEM image of the fracture surface of a bare
sample, stress level of 70 MPa, and 6 million cycles**

The pores of the cast material are observable in Figure 4–9. These pores increase the possibility of the local stress concentration which cause crack initiation [64], [65]. The multiple cracks shown in Figure 4–9 is initiated from these pores close to the surface which has higher stress level. This phenomenon of the initiation of the crack from the pores close to the surface has been reported for AZ91D cast alloy as well [66].

The scattering of the points presented in Figure 4–8 is higher than typical S-N curves for other materials. Comparison of these results with those of AZ31B extrude samples helps to illustrate the effect of porosities in the cast alloy of AZ31B. Figure 4–10 represents the S-N curve of AZ31B extrude samples performed by Ishihara et al. 2007 [20]. Both of parallel and vertical extrusion samples has higher fatigue limit than cast alloy.
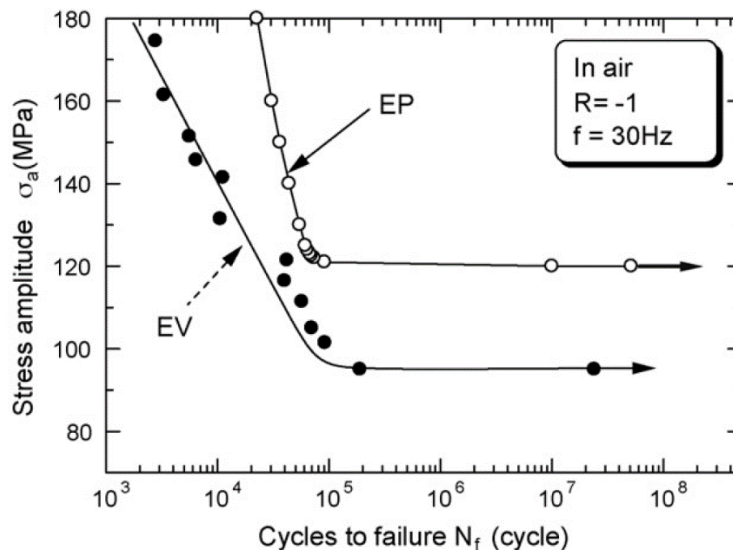


**Figure 4–10: S-N of AZ31B extrude in two direction [20]**

Comparing Fig 4-8 with Fig 4-10, there is considerably less scattering of the points in extrude alloy compared to cast alloy. One reason could be the non-uniform distribution of the porosities in cast alloys; for example, in some samples, these pores occur on or close to the surface and cause the crack initiation.

## 4.4 Fatigue test of cold spray coated samples

Fatigue tests were performed on 11 cold spray coated, polished samples over a period of about two weeks, with the same methods as those used for bare samples. A variety of load control stress levels were followed, and the up and down method was applied to reach the fatigue limit. The results are presented in Table 4-4.

**Table 4-4: The results of fatigue test on coated samples**

|  | Cycles | Stress | Result | Test duration |
|---|---|---|---|---|
| Different stress level from high stress to low stress | 43483 | 140 | Failure | ~ 7 minute |
|  | 21409 | 140 | Failure | ~ 3.5 minute |
|  | 258971 | 120 | Failure | ~ 43 minutes |
|  | 150043 | 120 | Failure | ~ 25 minutes |
|  | 1111879 | 100 | Failure | ~ 3 hours |
|  | 2690207 | 100 | Failure | ~ 7.5 hours |
| Up and down of the stress level regarding to run out result | 10054213 | 90 | **No failure** | ~ 28 hours |
|  | 4932096 | 95 | Failure | ~ 14 hours |
|  | 12854230 | 90 | **No Failure** | ~ 36 hours |
|  | 2352314 | 95 | Failure | ~ 6.5 hours |
|  | 10450231 | 90 | **No Failure** | ~ 29 hours |

The S-N curve and the low cycle regime line have also been extracted according to ASTM E739. They are presented in Figure 4–11 and Table 4-5, respectively, which also include the results for bare samples.
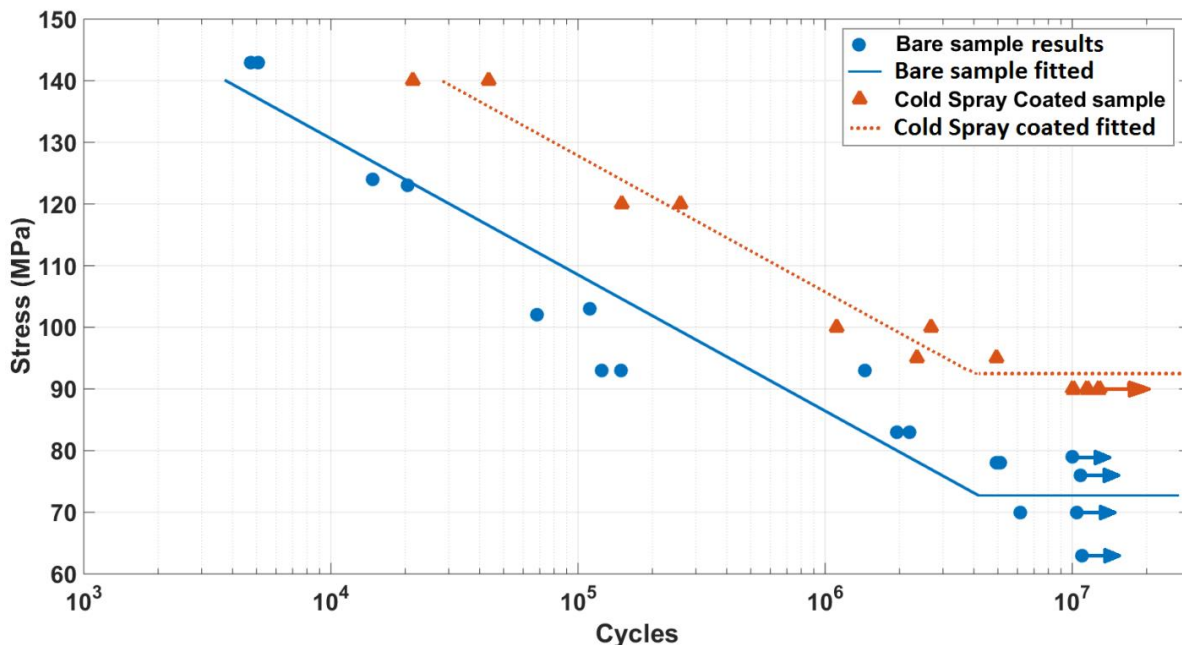


**Figure 4–11: S-N curve of bare and cold spray coated samples of AZ31B cast alloy**

**Table 4-5: Fatigue limit and low cycle regime line of bare samples and coated samples of AZ31B**

| | Fatigue limit | $R^2$ | Low-cycle regime line |
|---|---|---|---|
| **AZ31B cast alloy Bare** | 73.4±5.9 MPa | 0.899 | $-22.075\, Log\, N\ + 218.82$ |
| **AZ31B cast alloy cold spray coated by Al 7075** | 92±2.7 MPa | 0.951 | $-22.075\, Log\, N\ + 237.47$ |

These data demonstrate considerable improvement after cold spray coating from low-cycle to high-cycle fatigue testing. The fatigue limit was improved by around 25 percent. The cause of the improvement is another key point of the research, and the fracture surface images can provide more information about it. For this, two important regions were studied in further detail: the crack initiation region and the final fracture region. Figure 4–12 presents the fracture surfaces of the initial crack propagation region in a low-cycle fatigue sample. The crack initiation region of this sample at a stress level of 140 MPa is presented in Figure 4–13, as captured through two different SEM imaging methods.
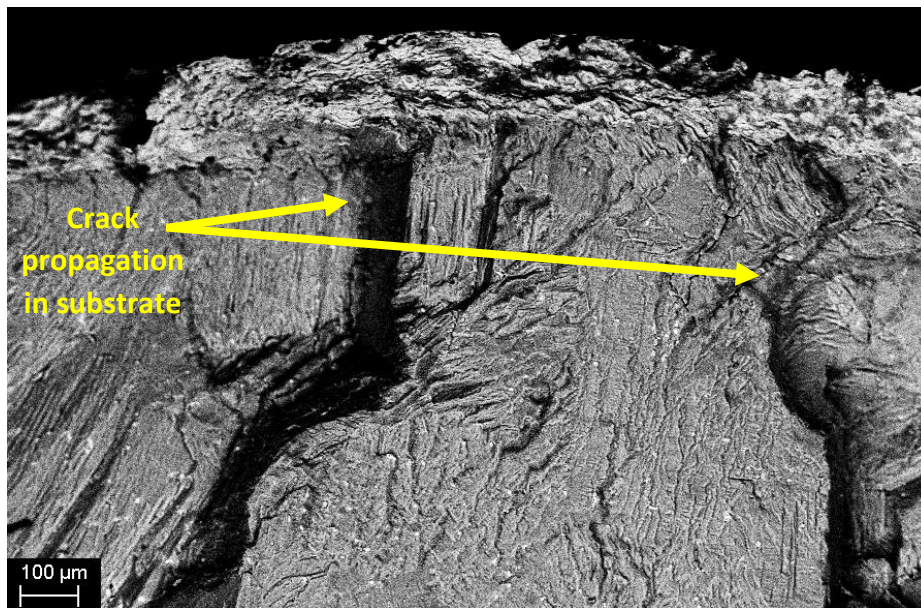


**Figure 4–12: Back scattered SEM image of the fracture surface of a low-cycle coated sample (140 MPa)**
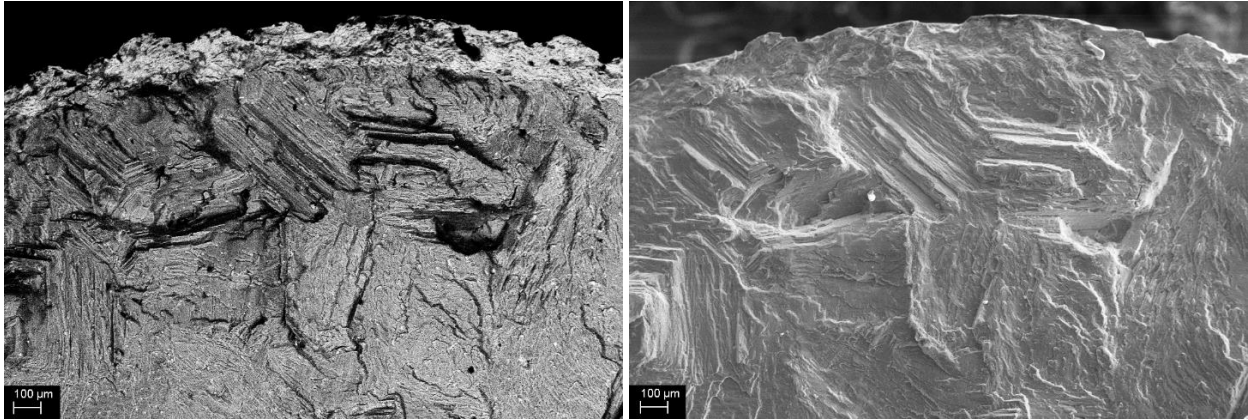
**Figure 4–13: Back scattered (left) and second electron beam (right) SEM images of the crack initiation region of a coated sample (140 MPa)**

Figure 4–13 shows no signs of delamination or crack in the interface region on the fracture surface in the vicinity of crack initiation zone. This confirms the quality of coat adhesion and removes any delamination-related failure as cause of failure.

SEM images were also taken of a high-cycle coated sample, and the final fracture region is presented in Figure 4–14. The other region of the fracture surface of this high-cycle sample is presented in Figure 4–15.

Important information that can be observed in the SEM images is that the crack propagation behaviour of the substrate in coated sample is similar to the crack propagation of bare samples but in the direction of the crack, there is no crack in the coat. In Figure 4–12 and Figure 4–15, this point is traceable. This indicates that the reason for the higher fatigue resistance in coated samples is that crack propagation will occur in the substrate, but its propagation will arrest or its growth rate will decrease when it reaches the coat, which has higher strength. Figure 4–15 shows that the crack was initiated on the substrate and propagate it but was arrested and did not lead to failure. The stopping of the crack propagation in the coat are at two different levels of stress.
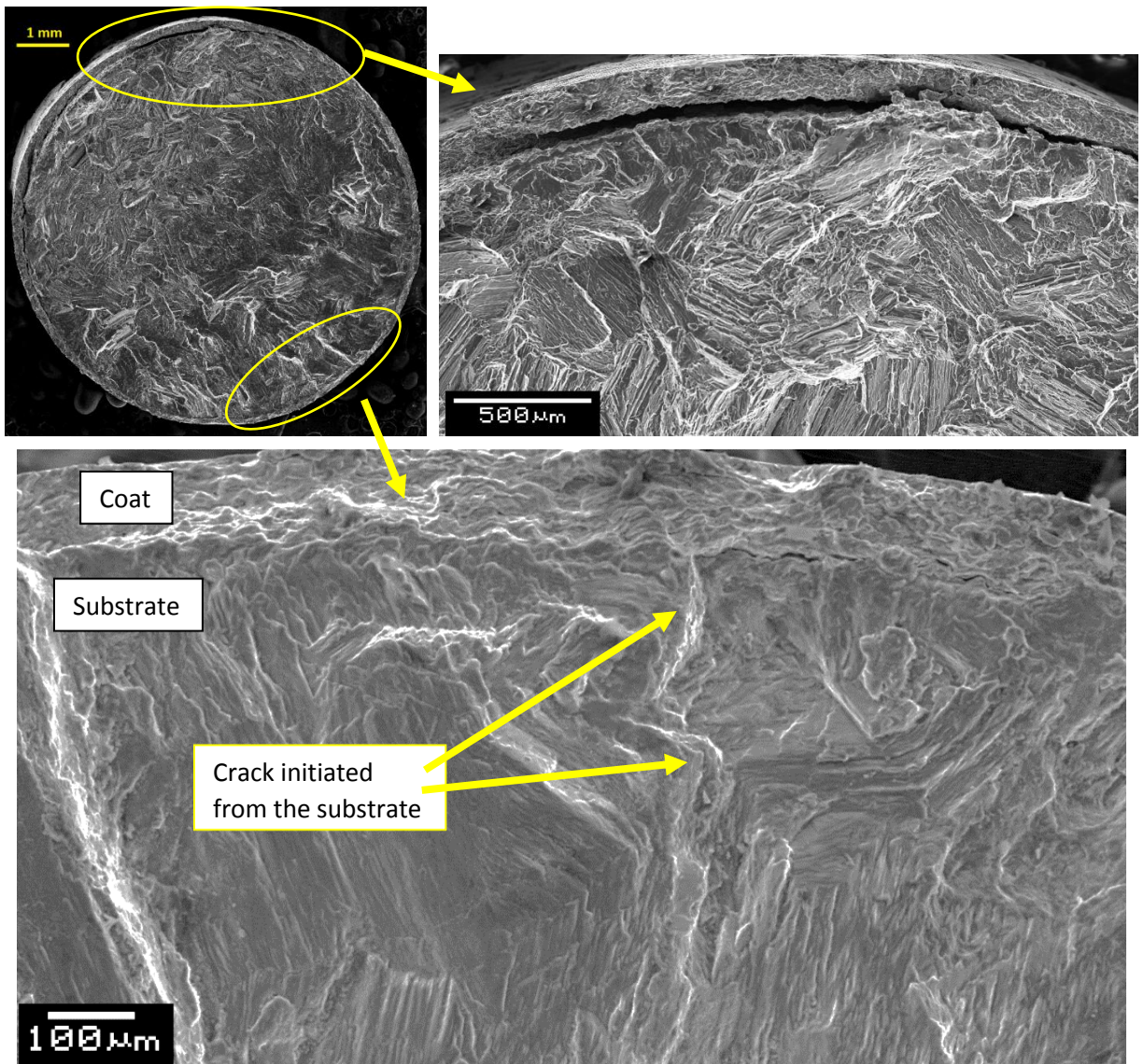
**Figure 4–14: SEM image of fracture surface of the sample of a high-cycle coated sample (95 MPa and 2.5 million cycles): final fracture region (above right) and initial crack region (bottom)**
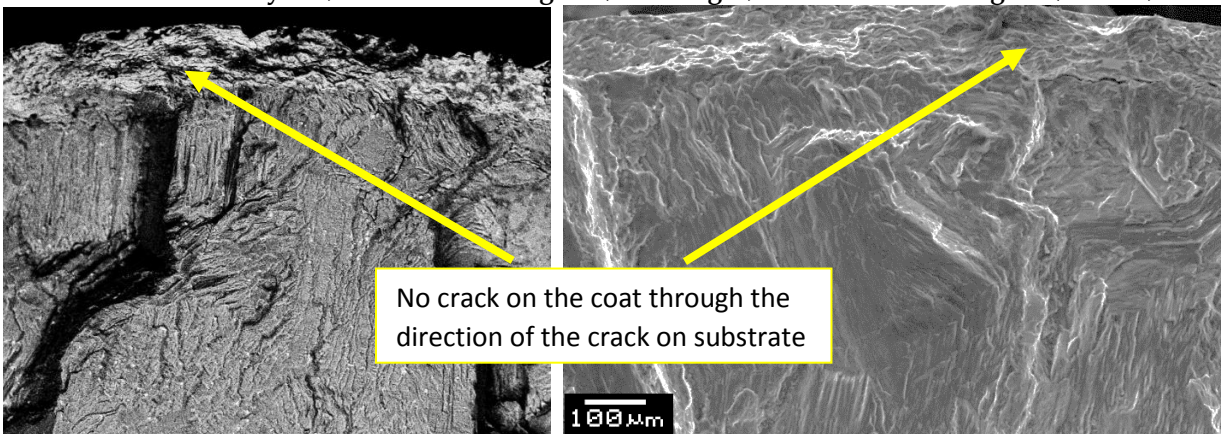


**Figure 4–15: SEM image of fracture surface of 140 MPa stress level sample (left) and 95 MPa stress level sample (right)**

The reason of the crack propagation in the material has been observed in fracture surfaces in different stress levels. All images prove that the cracks are initiated from the pores or propagate through the pores. This phenomenon is observable in both coated samples and un-coated samples. But the main difference between these two types is that the coating arrests the premature crack initiated from the substrate, as depicted by Figure 4–14.

The reason for overall fatigue improvement may be summarized as follows:

- The residual stress of the coat is compressive, measured by XRD and hole drilling measurement. The presence of residual stress reduces the maximum tensile stress at surface. This will in turn delay crack initiation and propagation in the coat.

- Higher hardness and fatigue resistance of the coat material in comparison to the substrate material had two effects in extending the life of the substrate. It acts as a barrier to crack propagation initiated from substrate. Also, the higher fatigue resistance of the coat provides the ability of taking higher level of stresses before any crack initiate and hence increasing the number of cycles to failure.

# Chapter 5  Corrosion-fatigue

As explained in the first two chapters, the corrosion tendency of magnesium alloys is higher than that of other alloys.   Therefore, corrosion prevention for magnesium alloys requires advanced, high-efficiency methods. Successful cold spray coating leads to higher fatigue resistance [36], but previous research has shown that it does not have effective improvement in corrosion-fatigue resistance [37].  Presence of magnesium and another metal in a corrosive environment usually causes anodic corrosion of the magnesium and this is referred to as, scarification of the anode to the cathode. Covering the surface of each of the two metals affects the corrosion rate. Because of this sensitivity of magnesium corrosion with another metal, a review of the effect of covering of the surface is presented.

By a very small cracks or damage of the anode coat, the corrosion rate of the anode is higher than the corrosion of cathode whose coat has small crack or damage. This difference is presented schematically in Figure 5–1. In these figures, metal 1 has a higher tendency and higher galvanic potential than metal 2. As explained above, metal 1 will be sacrificed for metal 2.
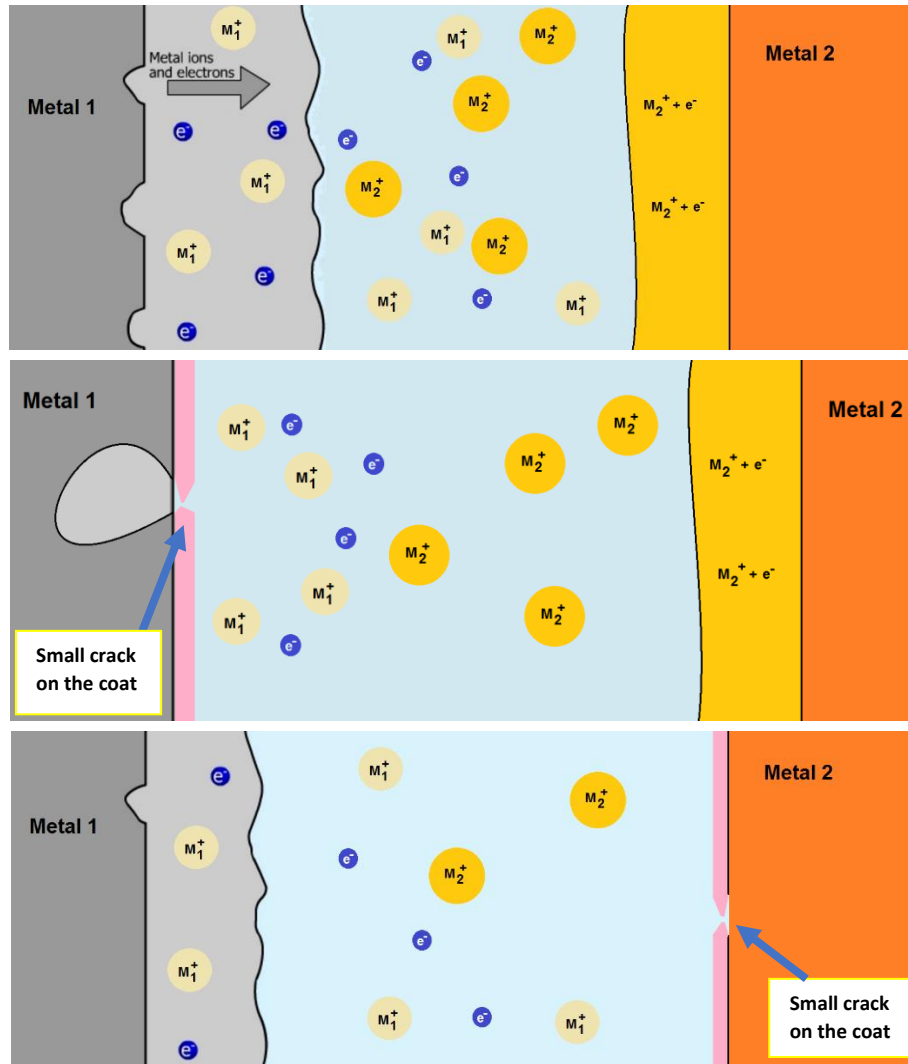
**Figure 5–1: Comparison of corrosion of two metals during coat damage**

According to research on the corrosion of magnesium, the dominant corrosion type is pitting corrosion [67]. Therefore, a method is required to provide a top coating, which has full covering for corrosion prevention for the magnesium and the cold spray coating. For this study painting method has been selected. Paint generally includes a pigment, which defines chemical reactions for corrosion prevention, and a resin, which prepares adhesion of the pigment particles on the surface of substrate [68]. The resin or the carrier of the paint is called the vehicle of the paint [69].

The poor corrosion-fatigue results of cold spray coating [37] and importance of full coverage of magnesium alloy which has high-tendency of corrosion justify the

necessity of a top coating on the cold spray coated sample. This combination of two types of coating is reported in other researches [70], [71].

## 5.1 Pigment selection (Zinc phosphate)

Many studies have been conducted to find the best coating method for corrosion prevention of magnesium alloys. Earlier studies [72] as well as recent ones [73] have been performed for pigment selection of the paint on magnesium alloys, and demonstrate that a variety of chemical salts are suitable for corrosion prevention. Zinc chromates has been identified as the best option [74]. A comprehensive study of the effectiveness of different pigments on preventing corrosion of magnesium substrate was performed in 1935 [69]; the results of this study are presented in Table 5-1. The tests were performed by immersing the magnesium alloy in a 3 % salt solution for two months.

Table 5-1: Comparison of the effect of different pigment
material on magnesium corrosion [69]

| Pigment material | Vehicle (carrier resin) | Failure percentage |
|---|---|---|
| Zinc chromate | Tung oil-phenolic | 2 |
| Zinc chromate | Oil-base natural resin | 25 |
| Red iron oxide | Oil-base ester-gum phenolic | 5 |
| Red iron oxide | Linseed oil | 100 |
| Red iron oxide | Oil-base synthetic | 65 |
| Black iron oxide | Tung oil-phenolic | 10 |
| Red iron oxide , zinc chromate | Tung oil-phenolic | 100 |
| Red iron oxide , zinc chromate | Oil-base natural resin | 85 |
| Red iron oxide , lead chromate | Linseed oil | 85 |
| Iron hydrate | Linseed oil | 100 |
| Lead chromate , red iron | Alkyd | 65 |
| Lithopone | Tung oil-phenolic | 25 |
| Titanox B | Oil-base alkyd | 80 |
| Red zinc | Linseed oil | 100 |
| Zinc dust | Linseed oil | 90 |
| Portland cement | Linseed oil | 5 |

As indicated by the results in Table 5-1, the best-quality corrosion resistance is provided by zinc chromate pigment. This qualification finding agrees with those of

other studies demonstrating that zinc chromate provides better corrosion resistance than other pigments [72]. However, in recent decades, the usage of chromate has been restricted because of its negative environmental impacts and carcinogenicity [75], [76]. Therefore, other chemical salts of zinc that do not have side effect should be selected. A pigment material that provides corrosion prevention close to that provided by zinc chromate pigment on a variety of substrates is zinc phosphate. This comparison has been performed in recent studies [77], [78], and [79]. In another study, researchers demonstrated that non-metal pigments (like metal salts) accompanied by zinc powder provide good corrosion resistance [80].

In recent studies on pigment materials, classification is based on application, substrate material, and preparation method. A more recent study on the corrosion of magnesium alloys confirmed that zinc phosphate provides good corrosion resistance for AZ91 alloy in a corrosive environment [81]. A common handbook of corrosion and prevention method [68] (page 322) states that:

*"Zinc phosphate coatings are widely used on steel, zinc, aluminum and sometimes cadmium, tin and magnesium surfaces."*

Based on the results of earlier and recent studies on pigment materials, as well as on environmental restrictions, zinc phosphate has been selected for this study as the pigment for top coating on the cold spray coated samples. The next important steps of the top coating preparation process are selection of the carrier resin and the deposition method of the paint on the samples' surface.

## 5.2 Electrostatic painting

Different types of coating deposition are available in the paint industry. Table 5-2 demonstrates the painting methods according to the handbook of paint technology [82]. The transfer efficiency values presented in the table represent the ratio of the coated paint to the total consumed paint.

**Table 5-2: Painting method and their transfer efficiency [82]**

| Coating method | Transfer efficiency |
|---|---|
| Air spray | 15~40 % |
| Airless spray | 20~50 % |
| Air-assisted airless spray | 30~60 % |
| High volume low pressure (HVLP) | 30~60 % |
| electrostatic airless | 40~70 % |
| electrostatic air spray | 40~80 % |
| Electrostatic air-assisted airless spray | 50~85 % |
| Electrostatic HVLP | 60~90 % |
| Electrostatic bell atomization | 70~95 % |
| Electrostatic disk atomization | 80~95 % |
| Electrostatic atomization | 95~98 % |

A study has been performed to improve the protective coating of magnesium alloys used in aircraft components [83]. The authors demonstrate that the best corrosion protection performance for two magnesium alloys (ZE41 and WE43) was provided by an electrostatic resin sealer painting. The superiority of e-coating vs other painting methods has been presented in another study [84], which demonstrated that the most uniform, full coverage painting was provided by electrostatic painting.

The electrostatic painting which is more commonly called e-painting or e-coating occurs as follows: the paint is deposited in the form of very small droplets, including the pigments and the vehicle (resin) on the surface of the substrate, by electrostatic force caused by opposite electrical charges of the substrate and the paint particles [82]. Figure 5–2 shows a schematic of the electrostatic painting process. The substrate will be completely covered by the paint in this method, even when the substrate is not directly in the pathway of the spray. Figure 5–3 presents another schematic view to show the coverage of the component under painting in the locations that are not subject to direct deposition of spray.
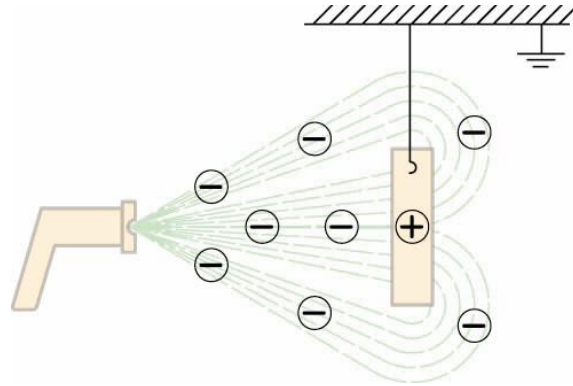
**Figure 5–2: Schematic view of electrostatic painting [85]**
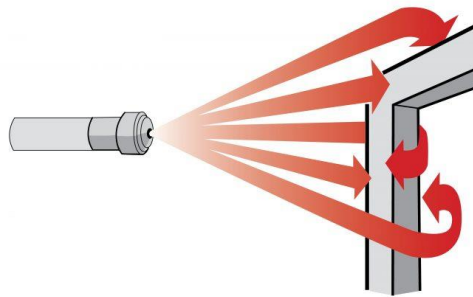


**Figure 5–3: Full coverage of the substrate in electrostatic painting [86]**

As explained above, the electrostatic coating (or e-painting) has been selected as the method for top coating of the cold spray coated samples in this study, and the top coat material selected is zinc phosphate. The selection of the paint resin was performed by the e-paint company. A number of companies were asked about their facilities and the possibility to carry out the painting according to other specifications, and the company MetoKote in Cambridge, Ontario was selected to perform the process.

## 5.3 Sample preparation

After two groups of fatigue testing, explained in Chapter Four, the remaining tests were classified in four conditions: corrosion-fatigue tests on bare samples, cold spray samples, e-painted samples, and cold spray coated e-painted samples. The two groups of samples used for e-painting were analogous to the group used in Chapter Four: the first group was 15 bare samples, and the second was 15 samples coated by

cold spray deposition with Al 7075; both groups were subject to the same fatigue test as applied in Chapter Four. The cold spray coated samples were polished in the same process explained in Chapter Four to reach the surface roughness. Samples in both groups were coated by MetoKote. According to the suggestion of MetoKote, the samples were hung on the painting line with a conductive hanger; Figure **5–4** shows the samples prepared by a hook hanger for electrostatic painting.



**Figure 5–4: Samples prepared for electrostatic painting. Bare samples (left) and cold spray coated polished samples (right)**

The e-painting process performed on the samples is explained in Figure **5–5**, and the recipe and the processes of each stage are presented in

Table **5-3**. Figure 5–6 shows an e-painted sample.
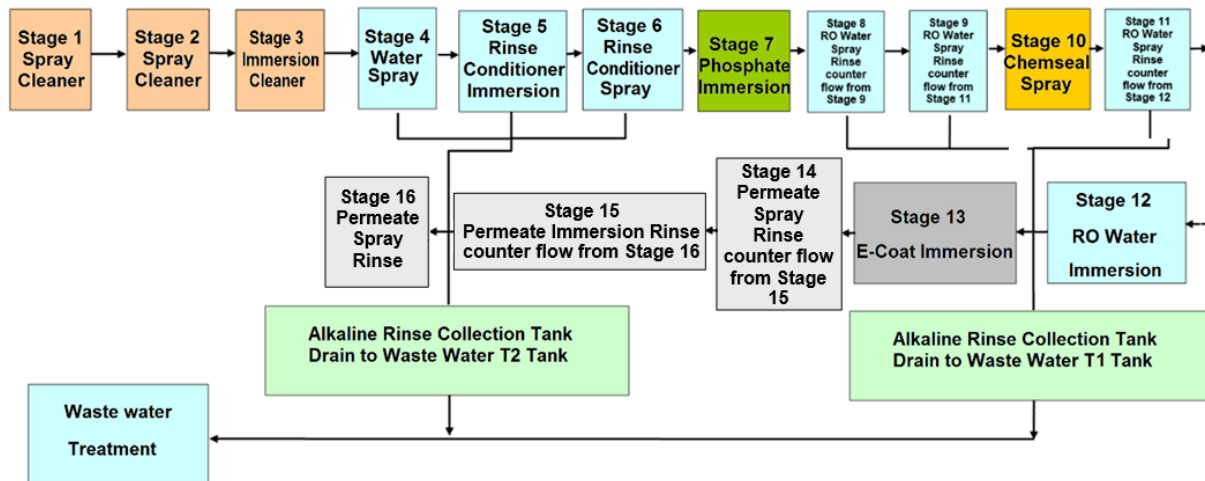


**Figure 5–5: The e-painting process of MetoKote company [87]**

57

**Table 5-3: The recipe of the e-painting process [87]**

|          | Description        | Method             |
|----------|--------------------|--------------------|
| Stage 1  | Cleaner            | Spray              |
| Stage 2  | Cleaner            | Spray              |
| Stage 3  | Cleaner            | Immersion          |
| Stage 4  | Rinse              | Spray              |
| Stage 5  | Conditioner        | Immersion          |
| Stage 6  | Conditioner        | Spray              |
| Stage 7  | Zinc Phosphate     | Immersion          |
| Stage 8  | Rinse              | Spray              |
| Stage 9  | Rinse              | Spray              |
| Stage 10 | Non-Chrome Sealer  | Spray              |
| Stage 11 | Rinse              | Spray              |
| Stage 12 | Rinse              | Immersion          |
| Stage 13 | Ecoat              | Immersion          |
| Stage 14 | Permeate           | Spray              |
| Stage 15 | Permeate           | Immersion          |
| Stage 16 | Permeate           | Spray              |
|          | Cure               | Oven (385 ± 10 F)  |



**Figure 5–6: E-painted sample**

## 5.4 Corrosion-fatigue test equipment

Corrosion-fatigue tests were performed by the rotating-bending test device explained in Chapter Four. A corrosive environment is required for these tests. Two common methods for preparing a corrosive environment are submerging specimen in a salt solution, and spraying the salt solution onto the specimen. A schematic view of the spraying method is presented in Figure 5–7. Both methods have been used by the researchers which are review below.
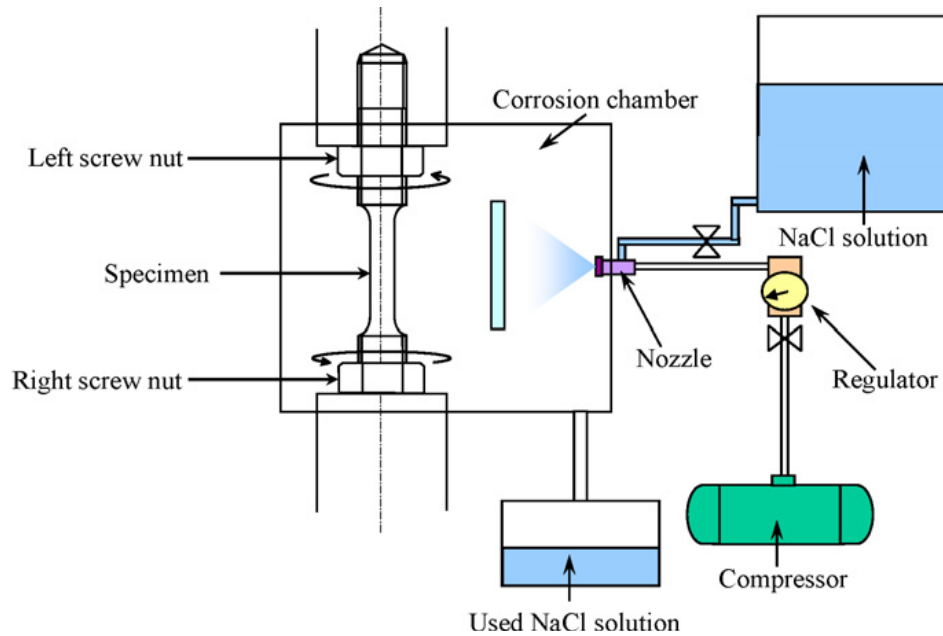
**Figure 5–7: Schematic view of spraying corrosion-fatigue test [88]**

Elizier et al, in 1998 [89] performed corrosion-fatigue tests on some magnesium alloys using a rotating-bending fatigue device and droplets of a 5 % of NaCl salt solution (equivalent to submerging). The frequency of their test was 40 Hz. Elizier et al. in 2001 [90] performed corrosion-fatigue tests on magnesium alloys, at a frequency of 30 Hz and using a 3.5 % salt solution. Unikovski et al. in 2003 [91] performed corrosion-fatigue tests on ZK60, AM50, and AZ31B with the same device using the rotating-bending method, and dropping a 3.5 % salt solution at a flow rate of 5 cc/min. The frequency of this test was also 30 Hz. They performed another tests in 2005 [92] on different magnesium alloys, following the same method explained, and the frequency and salt concentration were 30 Hz and 3.5 %, respectively. Mutoh et al. in 2008 [93] performed corrosion-fatigue tests on three types of magnesium alloys. The frequency and salt concentration were 20 Hz and 5 %, and the corrosive environment was prepared by spraying the solution. Nan et al. in 2008 [94] performed tests on rotating-bending magnesium alloys with the frequency, concentration, and flow rate of 30 Hz, 3

%, and 140 cc/min, respectively. Bhuiyan et al. in 2008 [95] performed a test by spraying a 5 % salt solution at a frequency of 20 Hz.

Another corrosion-fatigue test on magnesium alloy was performed by Elizier et al. in 2008 [96] by dropping a 3.5 % salt solution on a sample under 30 Hz of rotation speed. More recently, a test was performed at the University of Waterloo by Diab et al. [37] on AZ31B extruded alloy samples, by dropping a 3.5 % salt solution at a flow rate of 40 cc/min on a sample rotating with a frequency of 30 Hz. The summary of these studies are presented in Table 5-4.

**Table 5-4: The parameters used in corrosion-fatigue tests on magnesium alloys**

| Corrosion-fatigue Research | Test type | Test frequency (rotation speed) | Salt solution concentration | Solution flow rate |
|---|---|---|---|---|
| Elizier et al., 1998 [89] corrosion fatigue tests on some magnesium alloys | Spraying | 40 Hz | 5 % | 140 cc/min |
| Unikovski et al., 2003 [91] corrosion-fatigue tests on ZK60, AM50, and AZ31B | Dropping on specimen | 30 Hz | 3.5 % | 5 cc/min |
| Elizier et al. 2005 [92] magnesium alloys | Spraying | 30 Hz | 5 % | 140 cc/min |
| Mutoh et al., 2008 [93] three types of magnesium alloy | Dropping on specimen | 20 Hz | 5 % | 140 cc/min |
| Nan et al. 2008 [94] magnesium alloys | Spraying | 30 Hz | 5 % | 140 cc/min |
| Bhuiyan et al., 2008 [95] | Spraying | 20 Hz | 5 % | 140 cc/min |
| Elizier et al. 2008 [96] | Spraying | 20 Hz | 5 % | 140 cc/min |
| Buiyan et al., 2010 [88] | Spraying | 30 Hz | 5 % | 140 cc/min |
| Diab, 2017 [37] on AZ31B extrude | Dropping on specimen | 30 Hz | 5 % | 40 cc/min |

The above experiments were used to determine the three parameters to be used in this study: a solution concentration of 3.5 %, specimen rotational frequency of 30 Hz, and a flow rate of the salt solution of 40 CC/min. The corrosion-fatigue test device was prepared by placing a solution chamber around the sample and a flow of salt solution onto the sample over the duration of the test. Figure 5–8 shows the chamber and the specimen during the test.
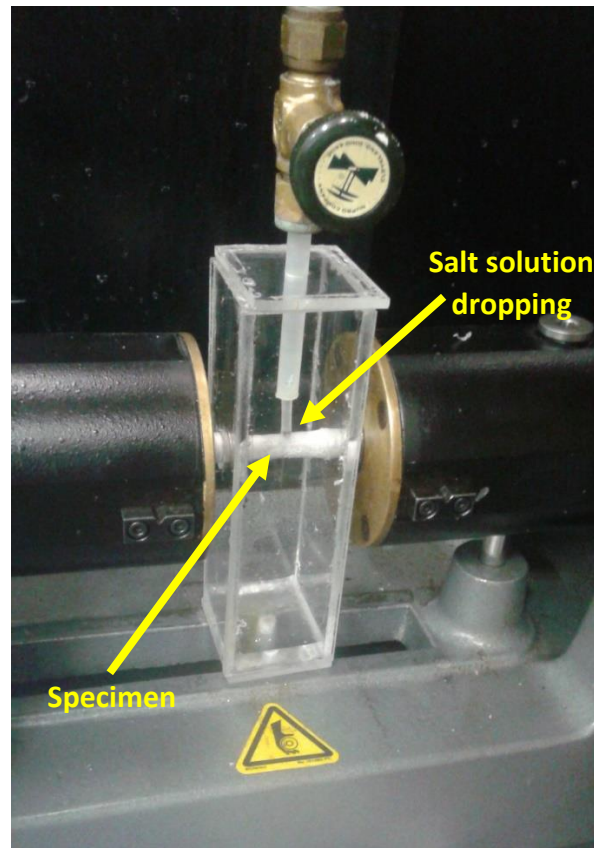


**Figure 5–8: Solution chamber around the specimen in corrosion-fatigue tests**

## 5.5 Corrosion-fatigue tests results

To enable a complete comparison, four tests were performed on different groups of samples, which are: bare samples, cold spray coated samples, e-painted samples, and cold spray coated e-painted samples. The results, represented by the number of cycles to fail versus stress level, are presented in Table 5-5. The results, presented as S-N curves, are presented in Figure 5–9. As in the fatigue tests explained in Chapter Four,

around the fatigue stress limit some trials were repeated, following the up and down method [61].

Table 5-5: Results of corrosion-fatigue tests

| Stress | Un-coated samples | | Cold spray coated samples | | E-painted samples | | E-painted cold spray coated samples | |
|---|---|---|---|---|---|---|---|---|
| | Cycle | Result | Cycle | Result | Cycle | Result | Cycle | Result |
| 140 | 1297 | Failure | 747 | Failure | 1907 | Failure | 5640 | Failure |
| 140 | 1345 | Failure | 1215 | Failure | 2066 | Failure | 8241 | Failure |
| 120 | 3215 | Failure | 4590 | Failure | 3749 | Failure | 25646 | Failure |
| 120 | 4224 | Failure | 12863 | Failure | 8349 | Failure | 33435 | Failure |
| 100 | 24832 | Failure | 171636 | Failure | 29251 | Failure | 1435472 | Failure |
| 100 | 22202 | Failure | 35581 | Failure | 25442 | Failure | 595231 | Failure |
| 90 | | | | | 465325 | Failure | 2618422 | Failure |
| 90 | | | | | 87335 | Failure | 4003622 | Failure |
| 80 | 121853 | Failure | 636398 | Failure | 3917189 | Failure | 10035185 | No Failure |
| 80 | 115509 | Failure | 223357 | Failure | 6049514 | Failure | 10032437 | No Failure |
| 80 | | | | | | | 10025528 | No Failure |
| 70 | | | | | 10012324 | No Failure | | |
| 70 | | | | | 10002651 | No Failure | | |
| 70 | | | | | 10002651 | No Failure | | |
| 60 | 902034 | Failure | 1129331 | Failure | | | | |
| 60 | | | 1564342 | Failure | | | | |
| 40 | 6033327 | Failure | 3336064 | Failure | | | | |
| 40 | 3251183 | Failure | 3723014 | Failure | | | | |
| Average stress of up and down tests | | | | | 74 MPa | | 84 MPa | |
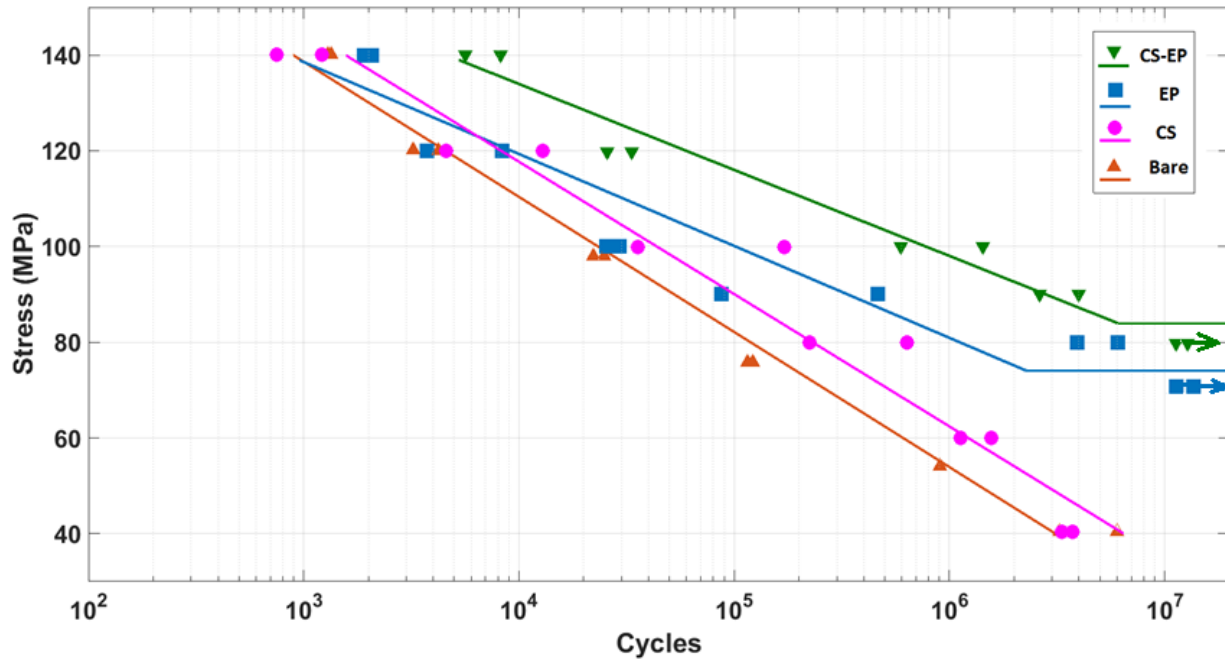
**Figure 5–9: S-N curves of corrosion-fatigue tests**

## 5.6 Fracture analysis

As presented in Table 5-5 and in Figure 5–9, the bare samples and cold spray coated samples did not reach the run out limit, while the two samples groups that had electrostatic painting reached the run out limits at 74 ± 5.4 MPa and 84 ±5.4 MPa, respectively. The cause of this behaviour is the question addressed in this section. The effect of the corrosive environment on the bare samples and cold spray coated samples are visually the same. Figure 5–10 shows the pitting corrosion on the surface of a cold spray sample at 40 MPa, which failed after 31 hours (3.1 million cycle). The cross section of the pitting region of the sample in Figure 5–10  is presented in Figure 5–11.

As observed in the images, pitting causes decrease in effective area which make the stress to rise. Also well they cause stress concentration which results in failure at lower stress level than those of samples without pitting which are tested in air or have been e-painted and tests in solution.
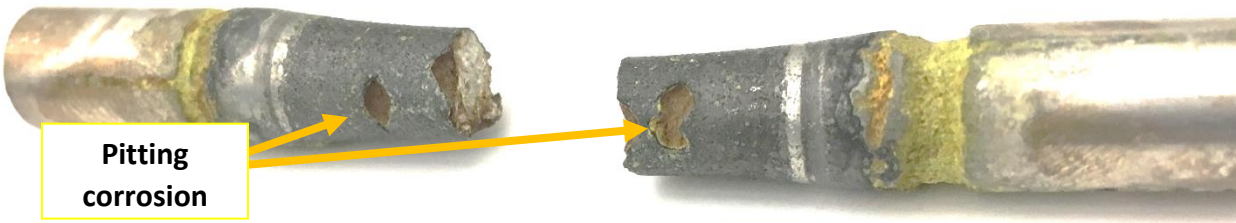
**Figure 5–10: The sample under 40 MPa stress after 31 hours of test**
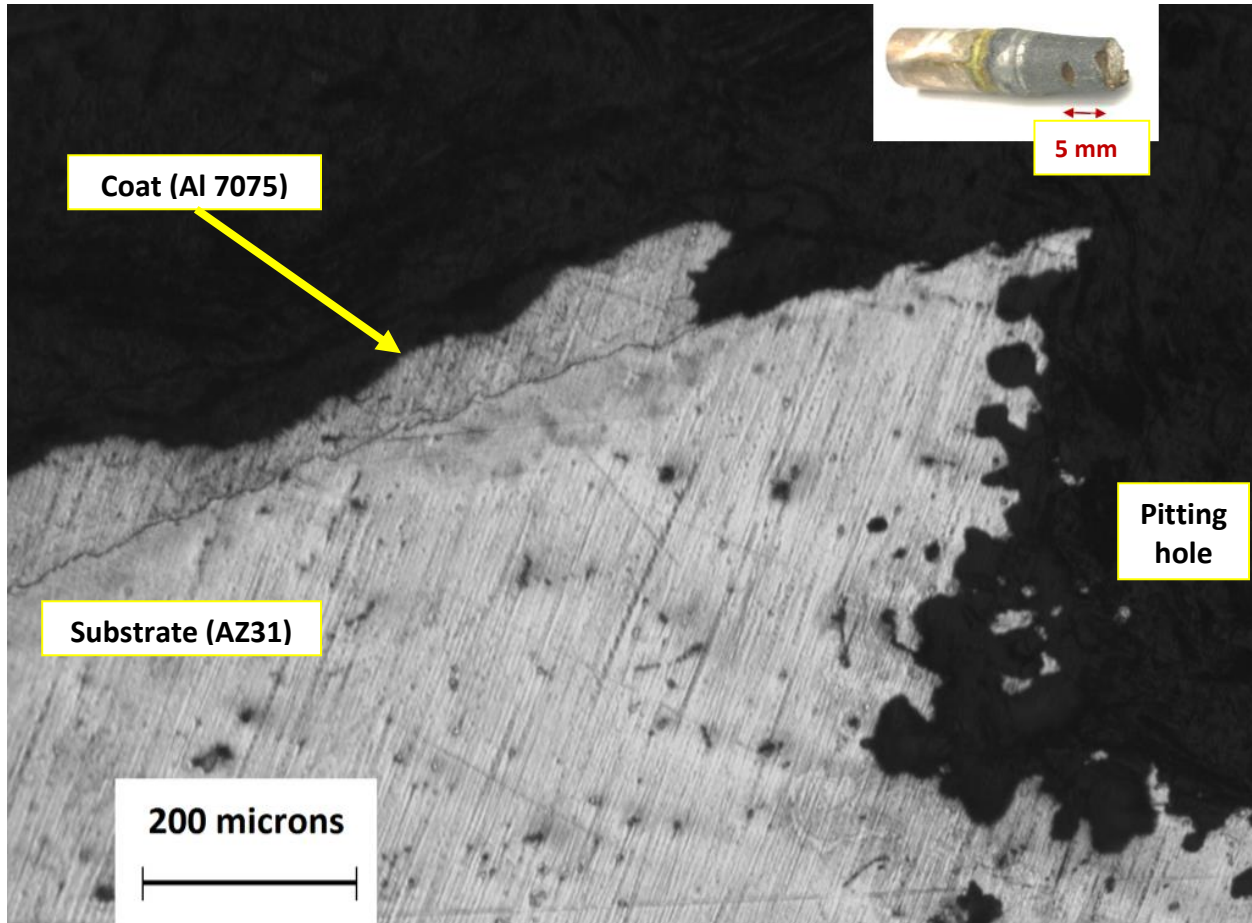


**Figure 5–11: The 5-mm cross-section of the fracture surface of the**
**sample under 40 MPa stress after 31 hours of test**

An SEM image of the fracture surface was captured for the cold spray coated sample at 100 MPa of stress level and at 171000 cycles (Figure 5–13). The duration of this test was 95 minutes. The penetration of the salt solution into the substrate is observable. Further details of the fracture surface are difficult to determine because corrosion of the surface occurred suddenly after the test. Figure 5–12 shows a decrease of the loading

area in pitting locations. Crack initiation from the pit in AZ31B extrude alloy is reported by Nan et al. [94]. Our research confirms that the crack initiation in AZ31B cast alloy is similar to extrude one and the crack propagation initiates from pits. In cold spray coated samples the crack process is the same to that of un-coated samples.



**Figure 5–12: Fracture surface happens in pitting holes location**
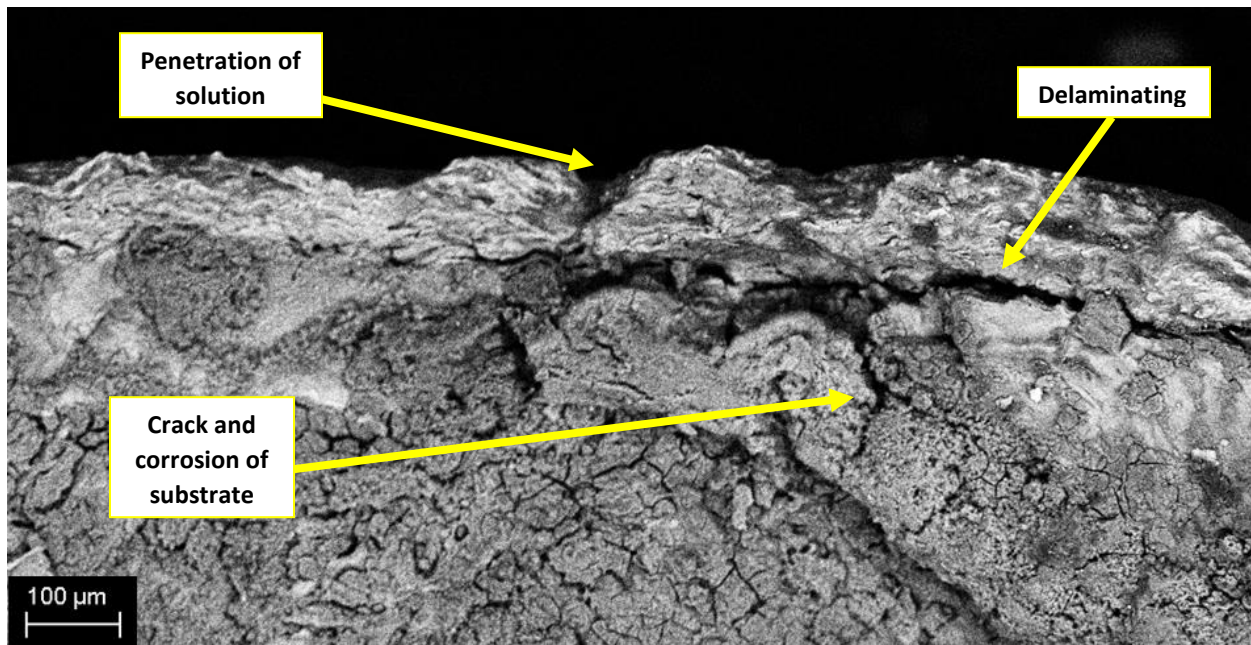


**Figure 5–13: SEM image of the fracture surface at a stress level of 100 MPa**

SEM images of e-painted samples were also captured. Figure 5–14 shows the cross section of an e-painted sample. The thickness of the paint is observable, and has been estimated to be 15 to 25 microns. Because of non-conductivity of the paint, the quality of the SEM images from the paint are lower than the quality of the images of the conductive regions and it looks like two layers of coat. Figure 5–15 shows a cross-section of a cold spray coated e-painted sample. These two images are taken after corrosion-fatigue test but in a region other than fracture surface.
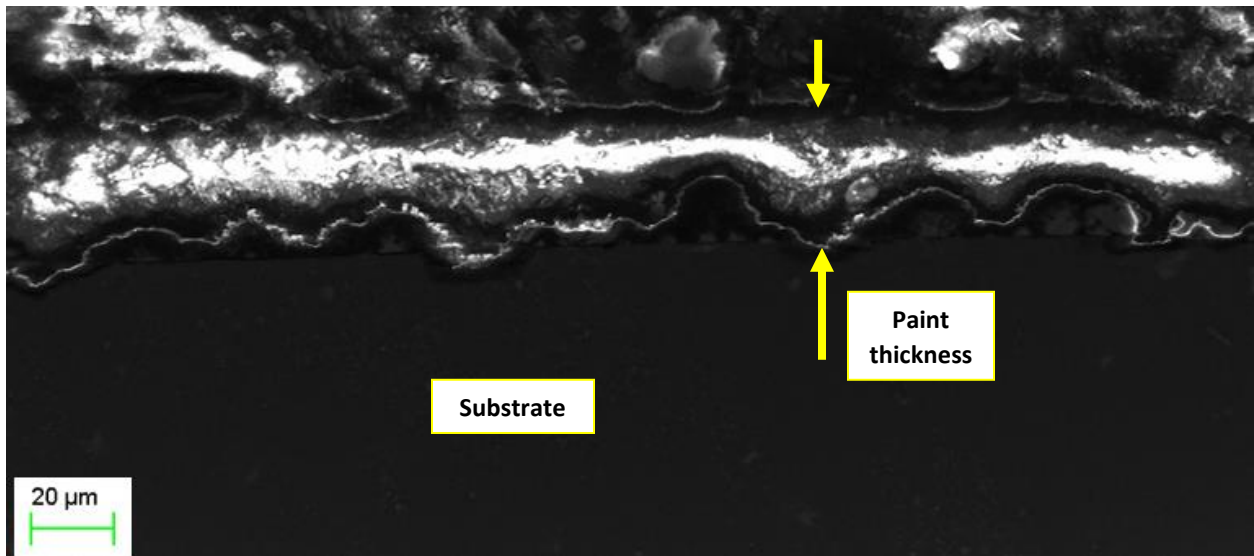


**Figure 5–14: SEM image of cross section of e-painted sample**
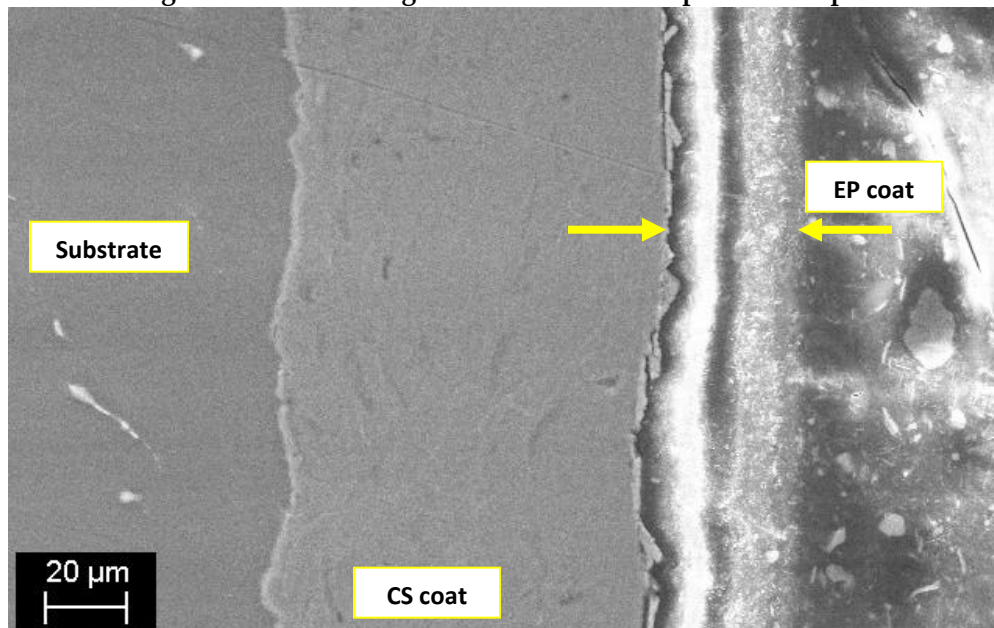


**Figure 5–15: Cross section of cold spray coated e-painted sample**

Both groups of e-painted samples reached the run out limit. The run out samples after 10 million cycles and 96 hours were visually the same as the samples before the test. Figure 5–16 represents the fracture surface of a cold spray coated e-painted sample under high stress. Corrosion suddenly occurs after fracture on the fracture surface and study of the crack is difficult on these images like Figure 5–16. But as presented in the literature [72], [68], [83], [84], the full coverage of the e-paint process and capability of zinc phosphate pigments on aluminum and magnesium substrate can be counted as the reason of improvement of e-painted samples. Full coverage of the sample like cross sections of Figure 5–14 and Figure 5–15 is observable in all samples reached to run-out limit.
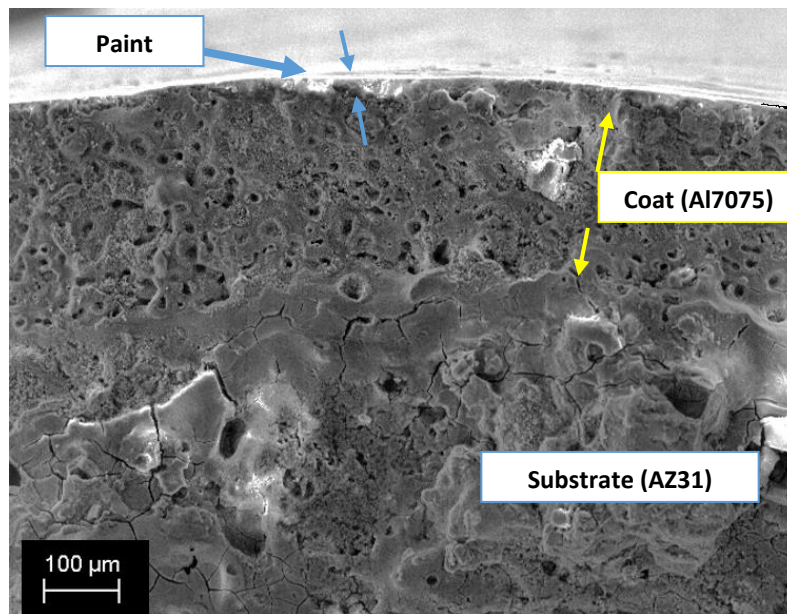


**Figure 5–16: Fracture surface of an e-painted sample, 140 MPa and 8000 cycles**

Reaching the run out limit of e-painted samples indicates that the electrostatic painting process is able to protect the magnesium alloy of AZ31B against corrosion. A sample after 10 million cycles and 80 MPa of stress level is shown in Figure 5–17. The difference between the fatigue limit of cold spray coated e-painted samples and e-painted samples (84 MPa vs 74 MPa) demonstrates the positive effect of cold spray on improving the fatigue resistance and the compatibility of cold spray coat of Al 7075 and

zinc phosphate painting. The fatigue limit of bare samples in air under fatigue testing (discussed in Chapter Four) and the corrosion-fatigue limit of e-painted samples are the same (74 MPa). This similarity demonstrates that the cause of failure in corrosion-fatigue test is related to the stress level and the ability of the paint to provide protection. Cold spray samples achieved higher fatigue resistance (test conducted in air) compared to bare samples. Also cold spray coated e-painted sample achieved higher corrosion-fatigue (test conducted in corrosive environment). The fatigue limit of cold spray sample in air was 92.5 MPa (compared to 73 for bare samples), and that of cold spray e-painted in corrosive environment was 84 MPa (compared to 74 for e-painted sample and no fatigue limit of bare samples). According to the effects of the cold spray process and residual stress, a hypothesis of the cause of this observed difference can be relieving of compressive residual stress during e-painting process which is discussed in the next chapter, and will continue to be investigated in future research. As an evaluation of the entire testing procedure, fitted S-N curves are presented in Figure 5–18.



**Figure 5–17: A cold spray coated e-painted sample after 10 million cycles in 80 MPa**
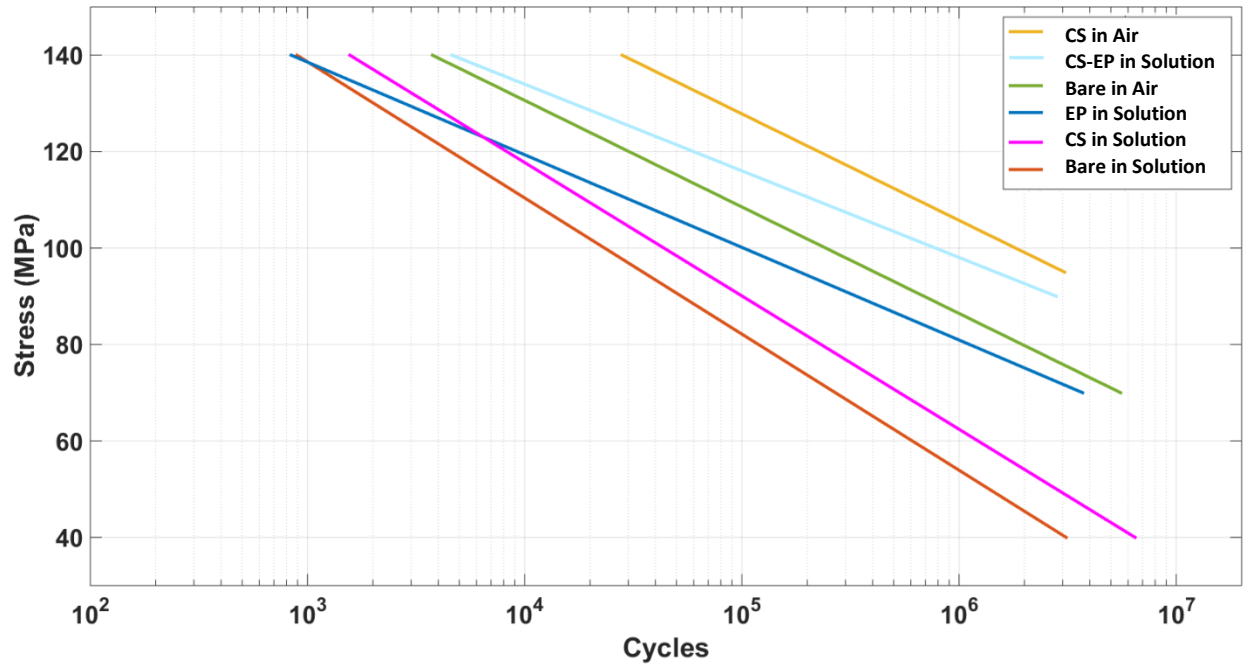
**Figure 5–18: S-N of six groups of fatigue tests in air and in solution**

# Chapter 6 Conclusion and future work

As presented in previous chapters, in this study, we performed cold spray deposition on the samples, and fatigue tests, corrosion fatigue tests, and characterization of the results. A summary of the findings of this study are represented below:

- Cold spray coating of Al 7075 powder on the substrate of AZ31B cast alloy has been successfully performed, with a low-pressure cold spray system (SST, P series Centerline). The coating thickness reached to expected amount, the porosity of the coat acceptable low, and the bonding force of the coat-substrate is strong enough comparable to other cold spray strength for both round samples and flat samples.

- Fatigue tests on round samples in two conditions: bare samples and cold spray coated samples, verified that a 25 % improvement in fatigue resistance occurred, as indicated by a 25 % improvement in fatigue limit and in the regime line of S-N curves (92 MPa vs. 73.4 MPa).

- SEM images of fracture surfaces in fatigue tests show that crack propagation in coated samples occurs in the substrates, however cracking does not occur to the same extent on the coat

- Zinc phosphate pigment with electrostatic painting has been successfully performed on the cold spray coated samples and bare samples.

- Both e-painted samples and cold spray coated e-painted samples reached the run-out limit in corrosion-fatigue tests in the corrosive environment, while neither bare samples nor cold spray coated samples reached the run-out limit in corrosion-fatigue tests.

- The fatigue limit of e-painted samples in the corrosive environment is the same as that of bare samples in air (73.4 MPa for bare samples in air and 74 MPa for e-painted samples in the corrosive environment).

- The fatigue limit of cold spray coated e-painted samples in the corrosive environment is less than that of cold spray coated samples in air (92 MPa for cold spray coated samples and 84 MPa for cold spray coated e-painted samples).

Of the above conclusions, the first, related to cold spray coating on magnesium, and the last, related to the difference in fatigue limit improvement between two conditions (before and after e-painting) lead to further questions, which should be investigate further in future research.

Cold spray of Al 7075 on AZ31B cast alloy with defined deposition parameters and conditions, explained in chapters three and four, has been performed. These are questions that need to be addressed in future research are identified below:

- Regarding the low deposition efficiency of Al 7075 as coating powder material, are there any other options to reach an

acceptable quality of coating on magnesium alloys? Regarding the lattice structure and behaviour in the cold spray process, the candidate material may be other aluminum alloys or other metals and alloys such as copper, steel, and titanium.

-What is the effect of the cold spray of Al 7075 on magnesium alloys other than AZ31B, such as AZ80, AZ91, and ZK60 with respect to criteria like bonding force, porosity, and fatigue resistance?

- How do changes in parameters and conditions of the coating process impact the results of the coat? If the coating process is performed using other parameters, for example higher pressure and temperatures typical of a high-pressure cold spray system, or using another carrier gas like helium, how does this influence results such as bonding force, fatigue resistance, and porosity? Is helium able to increase the deposition efficiency of Al 7075 to a more acceptable amount?

The difference in the resulting fatigue resistance under two conditions: before and after e-painting, introduces questions regarding the effect of the coating on fatigue resistance. The improvement is in part the result of the residual stress effect and in part due to the covering of the substrate surface with a stronger material. The area of research that should be pursued to determine the relative contributions of each of these factors are identified below:

- The level of improvement in fatigue resistance in coated sample following stress relief can separate the effect of hardness of coat effect on life from residual stress induced by coat on life.

- Measurements of residual stress in coated e-painted samples at different depths should be conducted, and a comparison of the results with the results of cold spray coated samples should be made. This can show if the e-paint process acted as stress relief process and relaxed the residual stresses.

More details of the coat and further study of the peening effect and the hardness distribution throughout the substrate and the coat are other promising approaches to investigate the bonding force and interface region. Chemical analysis of interference region will also help to elucidate more clearly the structure of the bonding force.

# References

[1] Magnesium Elektron Group, Magnesium Elektron, Manchester: Luxfer Group, 2012.

[2] M. K. Kulekci, "Magnesium and its alloys applications in automotive industry," *The International Journal of Advanced Manufacturing Technology,* vol. 39, p. 851–865, 2008.

[3] H. E. Friedrich and B. L. Mordike, Magnesium Technology Metallurgy, Design Data,Applications, Berlin: Springer-Verlag, 2006.

[4] H. Jahed and R. Ghelichi, "Residual Stresses and Fatigue Life Enhancement of Cold Spray," in *Modern Cold Spray*, New York, Springer, 2015, pp. 225-252.

[5] G. H. Farrahi, J. L. Lebrun and D. Couratin, "Effect of Shot Peening on Residual Stress and Fatigue Life of a Spring Steel," *Engineering Material and Structures Ltd,* vol. 18, pp. 211-220, 1995.

[6] H. Friedrich and S. Schumann, "Research for a "new age of magnesium" in the automotive industry," *Journal of Materials Processing Technology,* vol. 117, pp. 276-281, 2001.

[7] T. D. Gillespie, Fundamentals of Vehicle Dynamics, SAE, 1992.

[8] [Online]. Available: http://www.totalmotorcycle.com/MotorcycleFuelEconomyGuide.htm.

[9] [Online]. Available: http://www.boatingmag.com/calculating-fuel-consumption.

[10] [Online]. Available: http://www.fueleconomy.gov/.

[11] [Online]. Available: http://www.nrcan.gc.ca/node/7607.

[12] C. Bettles and M. Gibson, "Current wrought magnesium alloys: Strengths and weaknesses," *JOM,* vol. 57, pp. 46-49, 2005.

[13] H. Zenner and F. Renner, "Cyclic material behaviour of magnesium die castings and extrusions," *International Journal of Fatigue,* vol. 24, p. 1255–1260, 2002.

[14] N. D. DiMatteo, ASM Handbook Volume 19, Fatigue and Fracture, ASM, 1996.

[15] S. B. Behravesh, H. Jahed, S. Lambert and M. Chengji, "Constitutive Modeling for Cyclic Behavior of AZ31B Magnesium Alloy and its Application," *Advanced Materials Research,* vol. 891, pp. 809-814, 2014.

[16] K. Tokaji, M. Kamakura, Y. Ishiizumi and N. Hasegawa, "Fatigue behaviour and fracture mechanism of a rolled AZ31 magnesium alloy," *International Journal of Fatigue,* vol. 26, pp. 1217-1224, 2004.

[17] H.-K. Kim, Y.-I. Lee and C.-S. Chung, "Fatigue properties of a fine-grained magnesium alloy produced by equal channel angular pressing," *Scripta Materialia,* vol. 52, pp. 473-477, 2005.

[18] Y. Chino, T. Furuta, M. Hakamada and M. Mabuchi, "Fatigue behavior of AZ31 magnesium alloy produced by solid-state recycling," *Journal of Materials Science,* vol. 41, p. 3229–3232, 2006.

[19] S. Hasegawa, Y. Tsuchida, H. Yano and M. Matsui, "Evaluation of low cycle fatigue life in AZ31 magnesium alloy," *International Journal of Fatigue,* vol. 29, p. 1839–1845, 2007.

[20] S. Ishihara, Z. Nan and T. Goshima, "Effect of microstructure on fatigue behavior of AZ31 magnesium alloy," *Materials Science and Engineering,* vol. 468–470, p. 214–222, 2007.

[21] F. Yang, S. M. Yin, S.X. Li, Z.F. Zhang, S. X. Li and Z. F. Zhang, "Crack initiation mechanism of extruded AZ31 magnesium alloy in the very high cycle fatigue regime," *Materials Science and Engineering,* vol. 491, pp. 131-136, 2008.

[22] S. Begum, D. L. Chen, S. Xub and A. A. Luo, "Low cycle fatigue properties of an extruded AZ31 magnesium alloy," *International Journal of Fatigue,* vol. 31, p. 726–735, 2009.

[23] S. H. Park, S.-G. Hong, W. Bang and C. S. Lee, "Effect of anisotropy on the low-cycle fatigue behavior of rolled AZ31 magnesium alloy," *Materials Science and Engineering,* vol. 527, p. 417–423, 2010.

[24] R. G. Maev and V. Leshchynsky, Introduction to Low Pressure Gas Dynamic Spray, Wiley, 2008.

[25] A. Papyrin, V. Kosarev, S. Klinkov, A. Alkhimov and V. M. Fomin, Cold Spray Technology, Amsterdam: Elsevier, 2007.

[26] H. Assadi, F. Gärtner, T. Stoltenhoff and H. Kreye, "Bonding mechanism in cold gas spraying," *Acta Materialia,* vol. 51, pp. 4379-4394, 2003.

[27] M. Grujicic, C. L. Zhao, W. S. DeRosset and D. Helfritch, "Adiabatic shear instability based mechanism for particles/substrate bonding in the cold-gas dynamic-spray process," *Materials & Design,* vol. 25, p. 681–688, 2004.

[28] N. E. Dowling, Mechanical Behavior of Materials: Engineering Methods for Deformation, Fracture,

and Fatigue, Pearson, 2013.

[29] B. S. DeForce, T. J. Eden and J. K. Potter, "Cold spray Al-5% Mg coatings for the corrosion protection of magnesium alloys," *Journal of Thermal Spray Technology,* vol. 20, pp. 1352-1358, 2011.

[30] H. Bu, M. Yandouzi, C. Lu, D. MacDonald and B. Jodoin, "Cold spray blended Al + Mg17Al12 coating for corrosion protection of AZ91D magnesium alloy," *Surface and Coatings Technology,* vol. 207, p. 155–162, 2012.

[31] K. Spencer, D. M. Fabijanic and M. X. Zhang, "The use of Al–Al2O3 cold spray coatings to improve the surface properties of magnesium alloys," *Surface and Coatings Technology,* vol. 204, p. 336–344, 2009.

[32] Y. Fu, N. L. Loh, A. W. Batchelor, D. Liu, X. Zhu, J. He and K. Xu, "Improvement in fretting wear and fatigue resistance of Ti–6Al–4V by application of several surface treatments and coatings," *Surface and Coatings Technology,* vol. 106, p. 193–197, 1998.

[33] Y. J. Lee, S. C. Wu, J. H. Chen, M. T. Yeh, K. M. Lin and H. C. Lin, "Effects of Cold-Spray Coatings on the Corrosion Properties of AZ80 Magnesium Alloy," *Key Engineering Materials,* vol. 573, pp. 43-48, 2013.

[34] K. Spencer, V. Luzin, N. Matthews and M. X. Zhang, "Residual stresses in cold spray Al coatings: The effect of alloying and of process parameters," *Surface and Coatings Technology,* vol. 206, p. 4249–4255, 2012.

[35] A. Moridi, S. M. Hassani-Gangaraj, M. Guagliano and S. Vezzu, "Effect of Cold Spray Deposition of Similar Material on Fatigue Behavior of Al 6082 Alloy," in *Fracture and Fatigue, Volume 7, Proceedings of the 2013 Annual Conference*, Albuquerque, Springer, 2013, pp. 51-58.

[36] E. Kalatehmollaei, H. Mahmoudi-Asl and H. Jahed, "An asymmetric elastic–plastic analysis of the load-controlled rotating bending test and its application in the fatigue life estimation of wrought magnesium AZ31B," *International Journal of Fatigue,* vol. 64, p. 33–41, 2014.

[37] M. Diab, X. Pang and H. Jahed, "The effect of pure aluminum cold spray coating on corrosion and corrosion fatigue of magnesium (3% Al-1% Zn) extrusion," *Surface and Coatings Technology,* vol. 309, p. 423–435, 2017.

[38] R. Ghelichi, D. MacDonald, S. Bagherifard, H. Jahed, M. Guagliano and B. Jodoin, "Microstructure and fatigue behavior of cold spray coated Al5052," *Acta Materialia,* vol. 60, p. 6555–6561, 2012.

[39] L. F. Mondolfo, Aluminum Alloys: Structure and Properties, London: Butterworths, 1979.

[40] M. R. Rokni, C. A. Widener and G. A. Crawford, "Microstructural evolution of 7075 Al gas atomized powder and high-pressure cold sprayed deposition," *Surface and Coatings Technology,* vol. 251, p. 254–263, 2014.

[41] M. R. Rokni, C. A. Widener, G. A. Crawford and M. K. West, "An investigation into microstructure

and mechanical properties of cold sprayed 7075 Al deposition," *Materials Science and Engineering,* vol. 625, p. 19–27, 2015.

[42] C. C. S. S. S. Dept.. [Online]. Available: http://supersonicspray.com/en/.

[43] W.-Y. Li, H. Liao, H.-T. Wang, C.-J. Li, G. Zhang and C. Coddet, "Optimal design of a convergent-barrel cold spray nozzle by numerical method," *Applied Surface Science,* vol. 253, p. 708–713, 2006.

[44] K. Balani, T. Laha, A. Agarwal, J. Karthikeyan and N. Munroe, "Effect of carrier gases on microstructural and electrochemical behavior of cold-sprayed 1100 aluminum coating," *Surface and Coatings Technology,* vol. 195, p. 272–279, 2005.

[45] A. Pardo, M. C. Merino, P. Casajús, M. Mohedano, R. Arrabal and E. Matykina, "Corrosion behaviour of Mg–Al alloys with Al–11Si thermal spray coatings," *Materials and Corrosion,* vol. 60, p. 939–948, 2009.

[46] Centerline, "Manual of Cold Spray System," Centerline, Windsor, 2014.

[47] F. Podczeck, "A shape factor to assess the shape of particles using image analysis," *Powder Technology,* vol. 93, pp. 47-53, 1997.

[48] G. Shayegan, *Numerical Simulation of Residual Stress produced by Cold Spray on AZ31B,* Tehran: Science and Technology University of Iran, 2012.

[49] Q. Wang, K. Spencer, N. Birbilis and M.-X. Zhang, "The influence of ceramic particles on bond strength of cold spray composite coatings on AZ91 alloy substrate," *Surface and Coatings Technology,* vol. 205, pp. 50-56, 2010.

[50] E. Irissou, J.-G. Legoux, B. Arsenault and C. Moreau, "Investigation of Al-Al2O3 Cold Spray Coating Formation and Properties," *Journal of Thermal Spray Technology,* vol. 16, p. 661–668, 2007.

[51] T. Schmidt, F. Gärtner and H. Kreye, "Tabular Coating Tensile Test," Helmut Schmidt University, Hamburg, 2006.

[52] C. C. Berndt, "Tensile adhesion testing methodology for thermally sprayed coatings," *Journal of Materials Engineering,* vol. 12, p. 151–158, 1990.

[53] M. Couto, S. Dosta, M. Torrell, J. Fernández and J. M. Guilemany, "Cold spray deposition of WC–17 and 12Co cermets onto aluminum," *Surface and Coatings Technology,* vol. 235, p. 54–61, 2013.

[54] B. M. Gabriel, P. F. Leyman, D. J. Helfritch and V. K. Champagne, "Supersonic Particle Deposition for Repair and Corrosion Protection of Mg Gearboxes," 2009.

[55] S. Dosta, M. Couto and J. M. Guilemany, "Cold spray deposition of a WC-25Co cermet onto Al7075-T6 and carbon steel substrates," *Acta Materialia,* vol. 61, p. 643–652, 2013.

[56] D. J. Greving, J. R. Shadley and E. F. Rybicki, "Effects of coating thickness and residual stresses on the bond strength of ASTM C633-79 thermal spray coating test specimens," *Journal of Thermal*

*Spray Technology,* vol. 3, pp. 371-380, 1994.

[57] H. Mahmoudi-Asl, *The Effect of Residual Stress Induced by Cold Spray Coating on Fatigue Life of Magnesium Alloy, AZ31B,* Waterloo, 2011.

[58] F. P. Beer, E. R. Johnston and J. T. DeWolf, Mechanics of Materials, New York: McGraw-Hill, 2002.

[59] W. D. Callister and D. G. Rethwisch, Materials Science and Engineering, New York: Wiley, 2007.

[60] D. C. Montgomery, Design and Analysis of Experiments, New York: Wiley, 2013.

[61] R. D. Bruce, "An up-and-down procedure for acute toxicity testing," *Fundamental and Applied Toxicology,* vol. 5, p. 151–157, 1985.

[62] ASTM, "Standard Practice for Statistical Analysis of Linear or Linearized Stress-Life (S-N) and Strain-Life (ε-N) Fatigue Data," in *ASTM*, ASTM international, 2014.

[63] Instron, *RR Moore fatigue test machine Manual,* Instron, 2010.

[64] G. Atxaga, A. Pelayo and A. M. Irisarri, "Effect of microstructure on fatigue behaviour of cast Al–7Si–Mg alloy," *Materials Science and Technology,* vol. 17, pp. 446-450, 2001.

[65] H. Mayer, M. Papakyriacou, B. Zettl and S. E. Stanzl-Tschegg, "Influence of porosity on the fatigue limit of die cast magnesium and aluminium alloys," *International Journal of Fatigue,* vol. 25, p. 245–256, 2003.

[66] P. Cavaliere and P. P. De Marco, "Fatigue behaviour of friction stir processed AZ91 magnesium alloy produced by high pressure die casting," *Materials Characterization,* vol. 58, p. 226–232, 2007.

[67] H. Dong, Surface Engineering of Light Alloys: Aluminium, Magnesium and Titanium Alloys, CRC Press, 2010.

[68] M. Kutz, Handbook of Environmental Degradation of Materials, New York: William Andrew Publishing, 2005.

[69] A. W. WINSTON, J. B. REID and F. H. GROSS,, "Surface Preparation and Painting of Magnesium Alloys," *Industrial & Engineering Chemistry,* vol. 11, pp. 1333-1337, 1935.

[70] J. E. Gray and B. Luan, "Protective coatings on magnesium and its alloys — a critical review," *Journal of Alloys and Compounds,* vol. 336, p. 88–113, 2002.

[71] X. B. Chen, N. Birbilis and T. B. Abbott, "Review of Corrosion-Resistant Conversion Coatings for Magnesium and Its Alloys," *Journal of science and engineering,* vol. 67, pp. 1-16, 2011.

[72] R. I. Wray, "Painting Magnesium Alloy," *Industrial & Engineering Chemistry,* vol. 33, pp. 932-937, 1941.

[73] R.-G. Hu, S. Zhang, J.-F. Bu, C.-J. Lin and G.-L. Song, "Recent progress in corrosion protection of

magnesium alloys by organic coatings," *Progress in Organic Coatings,* vol. 73, p. 129–141, 2012.

[74] W. J. Wilson, "Method of coating magnesium metal to prevent corrosion," *US3537879,* 1970.

[75] J. M. Davies, "Lung cancer mortality among workers making lead chromate and zinc chromate pigments at three English factories," *Occupational and Environmental Medicine,* vol. 41, pp. 158-169, 1984.

[76] S. Langård and T. Norseth, "A cohort study of bronchial carcinomas in workers producing chromate pigments," *Occupational and Environmental Medicine,* vol. 32, pp. 62-65, 1975.

[77] M. Beiro, A. Collazo, M. Izquierdo, X. R. Nóvoa and Pérez, "Characterisation of barrier properties of organic paints: the zinc phosphate effectiveness," *Progress in Organic Coatings,* vol. 46, p. 97–106, 2003.

[78] M. Mahdavian and M. M. Attar, "Evaluation of zinc phosphate and zinc chromate effectiveness via," *Progress in Organic Coatings,* vol. 53, p. 191–194, 2005.

[79] A. C. Bastos, M. G. Ferreira and A. M. Simões, "Comparative electrochemical studies of zinc chromate and zinc phosphate as corrosion inhibitors for zinc," *Progress in Organic Coatings,* vol. 52, p. 339–350, 2005.

[80] A. Kalendová, P. Kalenda and D. Veselý, "Comparison of the efficiency of inorganic nonmetal pigments with zinc powder in anticorrosion paints," *Progress in Organic Coatings,* vol. 57, p. 1–10, 2006.

[81] L. Y. Niu, Z. H. Jiang, G. Y. Li, C. D. Gu and J. S. Lian, "A study and application of zinc phosphate coating on AZ91D magnesium alloy," *Surface and Coatings Technology,* vol. 200, p. 3021–3026, 2006.

[82] R. Talbert, Paint Technology Handbook, New York: CRC Press, 2008.

[83] M. Levy, F. Chang, B. Placzankis and R. Huie, "Improved protective schemes on magnesium aircraft alloys," in *NACE International*, 1996.

[84] T. Goldberg, L. Regenstein, J. Shearman, B. Anderson and L. Case, "Metal Painting and Coating Operations," NEWMOA, 2005.

[85] [Online]. Available: www.industrialsprayconcepts.co.uk.

[86] CHANDLER PAINTING COMPANY, [Online]. Available: http://arizonapaintingcompany.com/locations/chandler/.

[87] MetoKote, "MetoKote Manual".

[88] M. S. Bhuiyan, Y. Ostuka, Y. Mutoh, T. Murai and S. Iwakami, "Corrosion fatigue behavior of conversion coated AZ61 magnesium alloy," *Materials Science and Engineering,* vol. 527, p. 4978–

4984, 2010.

[89] A. Eliezer, E. M. Gutman, E. Abramov and E. Aghion, "Corrosion Fatigue and Mechanochemical Behaviour of Magnesium Alloys," *Corrosion reviews,* 1998.

[90] A. Eliezer, E. M. Gutman, E. Abramov and Y. Unigovski, "Corrosion fatigue of die-cast and extruded magnesium alloys," *Journal of Light Metals,* vol. 1, p. 179–186, 2001.

[91] Y. Unigovski, A. Eliezer, E. Abramov, Y. Snir and E. M. Gutman, "Corrosion fatigue of extruded magnesium alloys," *Materials Science and Engineering,* vol. 360, p. 132–139, 2003.

[92] A. Eliezer, J. Haddad, Y. Unigovski and E. M. Gutman, "STATIC AND DYNAMIC CORROSION FATIGUE OF Mg," *Materials and Manufacturing Processes,* pp. 75-88, 2005.

[93] Y. Mutoh, Z. Sajuri and M. S. Bhuiyan, "High Cycle Fatigue Behavior of Magnesium Alloys under Corrosive Environment," *Key Engineering Materials,* pp. 131-146, 2008.

[94] Z. Y. Nan, S. Ishihara and T. Goshima, "Corrosion fatigue behavior of extruded magnesium alloy AZ31 in sodium chloride solution," *International Journal of Fatigue,* vol. 30, p. 1181–1188, 2008.

[95] M. S. Bhuiyan, Y. Mutoh, T. Murai and S. Iwakami, "Corrosion fatigue behavior of extruded magnesium alloy AZ61 under," *International Journal of Fatigue,* vol. 30, p. 1756–1765, 2008.

[96] A. Eliezer, O. Medlinsky, J. Haddad and G. Ben-Hamu, "Corrosion fatigue behavior of magnesium alloys under oil environments," *Materials Science and Engineering,* vol. 477, p. 129–136, 2008.

[97] M. M. Avedesian and H. Baker, ASM Specialty Handbook: Magnesium and Magnesium Alloys, New York: ASM international, 1999.